Viral manipulation of a mechanoresponsive signaling axis disassembles processing bodies

Elizabeth L. Castle[1], Carolyn-Ann Robinson[2], Pauline Douglas[3, 5], Kristina D. Rinker[3, 4, 5], and Jennifer A. Corcoran[1, 2, 5, 6]

[1]Department of Microbiology and Immunology, Dalhousie University, Halifax, NS, Canada
[2]Current address, Microbiology, Immunology and Infectious Diseases Department and Charbonneau Cancer Research Institute, University of Calgary, Calgary, AB, Canada.
[3]Department of Physiology and Pharmacology, University of Calgary, Calgary, AB, Canada.
[4]Department of Chemical and Petroleum Engineering and Centre for Bioengineering Research and Education, University of Calgary, Calgary, AB, Canada.
[5]Charbonneau Cancer Institute, University of Calgary, Calgary, AB, Canada.
[6]Corresponding Author

Abstract

Processing bodies (PBs) are ribonucleoprotein granules important for cytokine mRNA decay that are targeted for disassembly by many viruses. Kaposi's sarcoma-associated herpesvirus is the etiological agent of the inflammatory endothelial cancer, Kaposi's sarcoma, and a PB-regulating virus. The virus encodes Kaposin B (KapB), which induces actin stress fibres (SFs) and cell spindling as well as PB disassembly. We now show that KapB-mediated PB disassembly requires actin rearrangements, RhoA effectors and the mechanoresponsive transcription activator, YAP. Moreover, ectopic expression of active YAP or exposure of ECs to mechanical forces caused PB disassembly in the absence of KapB. We propose that the viral protein KapB activates a mechanoresponsive signaling axis and links changes in cell shape and cytoskeletal structures to enhanced inflammatory molecule expression using PB disassembly. Our work implies that cytoskeletal changes in other pathologies may similarly impact the inflammatory environment.

Importance

For the first time, we demonstrate that processing bodies (PBs), cytoplasmic sites of RNA decay, are regulated by mechanical signaling events that alter actin dynamics. Using the overexpression of a viral protein called KapB, known previously to mediate PB disassembly, we show that actin stress fibers (SFs) and the mechanoresponsive transcription factor, YAP, are required for PB loss. We also show that other established mechanical signals (shear stress or stiff extracellular matrix) that lead to the formation of SFs and activate YAP also cause PB disassembly. This is important because it means that KapB activates, from the inside out, a pathway that links cell shape to post-transcriptional gene regulation via cytoplasmic PBs.

Introduction

Cells are exposed to a variety of environments and they respond to changes in external force by adjusting internal tension. These mechanical cues can be transmitted to the cell through changes to extracellular contact nodes (focal adhesions) and contractile actomyosin structures to maintain tension homeostasis (Friedland, Lee, and Boettiger 2009; Kong et al. 2009; del Rio et al. 2009; Grashoff et al. 2010; reviewed in Finch-Edmondson and Sudol 2016). Actin stress fibres (SFs) are cytoskeletal structures composed of thick actin bundles, often associated with focal adhesions (Vallenius 2013), that are force-responsive, maintaining cytoskeletal integrity in changing mechanical environments (Burridge and Guilluy 2016). SF formation is coordinated by the GTPase, RhoA; it activates the formin, mammalian diaphanous protein-1 (mDia1) to promote actin filament growth and Rho-associated coiled-coil kinase (ROCK) to promote actomyosin contractility through non-muscle myosin II (Watanabe et al. 1997; Amano et al. 1997; Kimura et al. 1996). These RhoA-effectors act together to promote the formation of contractile and stable actin filaments in response to mechanical and chemical stimuli (Watanabe et al. 1999).

External forces elicit a cascade of signals using actin as force transducers to alter gene expression. Activated serum response factor (SRF) transcription responds to actin polymerization (reviewed in Chai and Tarnawski 2002). SRF activation is negatively regulated by the cytoplasmic concentration of monomeric G-actin (Sotiropoulos et al. 1999). However, inducers of filamentous actin (e.g. active RhoA) deplete G-actin levels leading to SRF nuclear translocation and transcription (Sotiropoulos et al. 1999). A more recent example is the mechanoresponsive transcriptional coactivator Yes-associated protein (YAP), whose activity can be controlled by cell shape and cytoskeletal structure (Dupont et al. 2011; Wada et al. 2011; Halder, Dupont, and Piccolo 2012; Yu et al. 2012). YAP is nuclear and active in response to low cell-cell contact (Zhao et al. 2007), high stiffness of the extracellular matrix (ECM) (Dupont et al. 2011), in shear stress due to fluid flow (K.-C. Wang et al. 2016; Nakajima et al. 2017; Lai and Stainier 2017; H. J. Lee et al. 2017; Huang et al. 2016), or after G-protein coupled receptor (GPCR) activation (Yu et al. 2012). Most of these signals induce the activity of RhoA and promote the formation of SFs, (Noria et al. 2004; Lee and Kumar 2016), implicating actin cytoskeletal structures as requisite intermediates for YAP activation.

Nuclear YAP associates with its coactivators to mediate transcription of genes involved in cell proliferation, differentiation, survival and migration (Halder, Dupont, and Piccolo 2012).

57 Consistent with this, nuclear YAP is often pro-tumourigenic and drives progression of many
58 oncogenic traits in a variety of cancers. These include the induction of cell stemness (Panciera et
59 al. 2016), altered metabolism (C. Yang et al. 2018), cancer cell invasion/vascular remodeling
60 (Calvo et al. 2013; Liu et al. 2018; Kimura et al. 2020), and altered growth and proliferation
61 (Kapoor et al. 2014; Zanconato et al. 2015; Jang et al. 2017). Kaposi's sarcoma (KS) is an
62 endothelial cell (EC) cancer that is strongly linked to Kaposi's sarcoma-associated herpesvirus
63 (KSHV) (Chang et al. 1994; Russo et al. 1996; Zhong et al. 1996; Ganem 1997). KSHV
64 establishes persistent, life-long infection of its human host, and displays two types of infection,
65 latent and lytic. In KS, the majority of the tumour ECs are latently infected while lytic replication
66 is rare; in part, because these cells die as a result of viral replication (Boshoff et al. 1995; Staskus
67 et al. 1997; Umbach et al. 2010; Speck and Ganem 2010; Arias et al. 2014). That said, during
68 their short lifetime lytic cells expel progeny virus and secrete large quantities of pro-
69 inflammatory and angiogenic molecules, making even infrequent lytic replication an important
70 driver of KS. A key contributor to this secretory phenotype is the constitutively active viral G
71 protein-coupled receptor (vGPCR), a lytic viral protein (Montaner et al. 2006; Corcoran et al.
72 2012). Despite the paracrine contributors like vGPCR, the few gene products that are expressed
73 during the KSHV latent cycle are central for viral tumourigenesis. Many features of *in vivo* KS
74 are recapitulated by *in vitro* latent infection of primary ECs, or ectopic expression of individual
75 KSHV latent genes, including enhanced proliferation and an elongated or 'spindled' morphology
76 characteristic of KS. Spindling is induced by two KSHV latent genes, vFLIP (Grossmann et al.
77 2006) and Kaposin B (KapB; (Corcoran, Johnston, and McCormick 2015)). Spindled cells also
78 secrete a variety of proinflammatory cytokines and angiogenic factors, to further promote tumour
79 progression through inflammatory cytokine production (Ensoli 1998; Ciufo et al. 2001; Naranatt
80 et al. 2003; Grossmann et al. 2006; Ojala and Schulz 2014). However, no information exists to
81 demonstrate YAP involvement in KSHV latency, despite the fact that the vGPCR has been
82 shown to activate YAP during KSHV lytic infection (Liu et al. 2015).
83 One way that KSHV latency promotes the pro-inflammatory and pro-tumourigenic KS
84 microenvironment is via KapB-mediated disassembly of cytoplasmic ribonucleoprotein granules
85 called processing bodies (PBs) (Corcoran, Johnston, and McCormick 2015). PBs are involved in
86 many RNA regulatory processes such as RNA silencing, nonsense-mediated decay and mRNA
87 decay and translational suppression of mRNA (Eulalio, Behm-Ansmant, and Izaurralde 2007,

88 Horvathova et al. 2017, Tutucci et al. 2018, Wilbertz et al. 2019, Hubstenberger et al. 2017). We
89 and others have shown that PBs are the major site for the translational suppression or constitutive
90 decay of human mRNAs that code for potent regulatory molecules such as proinflammatory
91 cytokines (Franks and Lykke-Andersen 2007; Corcoran, Johnston, and McCormick 2015; Vindry
92 et al. 2017; Blanco et al. 2014). There are ~4500 of these transcripts, all of which bear
93 destabilizing AU-rich elements (AREs) in their 3'-untranslated regions (3'-UTRs) (Shaw and
94 Kamen 1986; Shyu, Greenberg, and Belasco 1989; Chen and Shyu 1995; Winzen et al. 1999;
95 Stoecklin, Mayo, and Anderson 2006; Franks and Lykke-Andersen 2007; Bakheet, Williams,
96 and Khabar 2006; Bakheet, Hitti, and Khabar 2017). PB abundance and composition is
97 extremely dynamic and responds to cellular stress (Sheth 2003; Kedersha and Anderson 2007;
98 Aizer et al. 2008; Takahashi et al. 2011). Specifically, activation of the stress-responsive
99 p38/MK2 MAP kinase pathway by KapB elicits PB disassembly and prevents constitutive ARE-
100 mRNA turnover or translation suppression (Winzen et al. 1999; Docena et al. 2010; Corcoran et
101 al. 2012; Corcoran and McCormick 2015; Corcoran, Johnston, and McCormick 2015). This is an
102 important yet underappreciated regulatory mechanism that fine tunes the production of potent
103 proinflammatory cytokines and angiogenic factors in KS.
104 Though PBs are dynamic and stress-responsive, the precise signaling events that lead to
105 PB assembly or disassembly are not well understood. We showed previously that KapB binds
106 and activates MK2, which then phosphorylates hsp27, complexes with p115RhoGEF, and
107 activates RhoA to elicit PB disassembly (Corcoran, Johnston, and McCormick 2015; Garcia et
108 al. 2009; McCormick and Ganem 2005). While it is well-established that RhoA coordinates SF
109 formation (Ridley and Hall 1992; Watanabe et al. 1999; Schmitz et al. 2000; Hotulainen and
110 Lappalainen 2006), the precise mechanism of how RhoA promotes PB disassembly is not
111 appreciated (Corcoran, Johnston, and McCormick 2015; Takahashi et al. 2011). In an effort to
112 better understand the regulation of PB disassembly by KapB and RhoA, we began by targeting
113 downstream RhoA effectors reported to promote SF formation to determine if the proteins
114 known to mediate cytoskeletal remodeling were also necessary for PB disassembly. We reasoned
115 that at some point we would be able to uncouple the signaling events that led to SFs from those
116 that led to PB disassembly. We were not. We now present data that conclusively shows KapB-
117 mediated PB disassembly is dependent not only on RhoA, but on cytoskeletal structures,
118 actomyosin contractility and the presence of the mechanoresponsive transcription transactivator,

119 YAP. We also present the first evidence of the involvement of YAP in the tumourigenic
120 phenotypes induced by a KSHV latent gene, KapB. We also extend these studies beyond their
121 impact on viral tumourigenesis, by determining the mechanical regulation of PB dynamics in the
122 absence of KapB expression, and show that induced cell contractility, cytoskeletal structures and
123 active YAP all precede PB disassembly. Using a viral protein from an oncogenic virus, we have
124 discovered a mechanoresponsive signaling pathway that transduces signals from cell shape and
125 cytoskeletal structures to YAP to control PBs, post-transcriptional regulators of cellular gene
126 expression.
127
128 **Results**
129 **RhoA effectors controlling SF formation are required for PB disassembly**
130 We previously showed that KapB-mediated PB disassembly required RhoA (Corcoran,
131 Johnston, and McCormick 2015). In this work, we investigated whether downstream RhoA
132 effectors known to control SF formation also control PB disassembly. Mammalian diaphanous
133 protein 1 (mDia1) and Rho-associated coiled-coil kinase (ROCK) are considered the main
134 coordinators of RhoA-mediated SF formation (Watanabe et al. 1999; Tojkander, Gateva, and
135 Lappalainen 2012). mDia1 is a formin that promotes actin filament polymerization (Watanabe et
136 al. 1999). To examine whether mDia1 was required for KapB-mediated PB disassembly, we
137 designed short hairpin RNAs (shRNAs) to silence mDia1 mRNA. KapB- and vector- expressing
138 human umbilical vein endothelial cells (HUVECs) were transduced with mDia1-targeting
139 shRNAs and selected. Silencing efficacy was confirmed with immunoblotting (Fig 1A). PB
140 analysis was performed using CellProfiler to quantify immunofluorescence images stained for
141 the hallmark PB-resident protein, Enhancer of mRNA decapping 4 (EDC4), as described in
142 detail in the methods (J. H. Yu et al. 2005; Kedersha et al. 2008). Knockdown of mDia1
143 increased PBs in KapB-expressing cells (Fig 1B, D). mDia1-sh1 showed a greater increase in
144 PBs in comparison to mDia1-sh2 (Fig 1B), and also increased PBs in vector control cells, likely
145 because mDia1-sh1 reduced protein expression by 90% whereas mDia1-sh2 reduced it by 40-
146 50% (Fig 1A). To separate how silencing of mDia impacted baseline turnover of PBs from how
147 silencing impacts KapB-mediated PB disassembly, we calculated the ratio of PBs per cell in
148 KapB-expressing cells and normalized to PBs per cell in the control. This is important because
149 this calculation shows whether KapB is still able to disassemble PBs, relative to vector, in the

150 context of mDia silencing. If the ratio is ≥1 after sh-mDia treatment, it indicates that KapB is no
151 longer able to disassemble PBs in comparison to the vector control, and that mDia contributes
152 directly to KapB-mediated PB disassembly. Conversely, if the ratio is ~ 0.4 to 0.6, it indicates
153 that KapB can still disassemble PBs even in the context of sh-mDia treatment. In this case, we
154 determined that silencing using both mDia1-sh1 and mDia1-sh2 restored the PB ratio in
155 KapB:Vector cells to ~1, indicating that the ability of KapB to disassemble PBs is lost after
156 mDia silencing and that this is a specific effect (Fig 1C). We note that this ratio will be reported
157 in subsequent figures for every RNA silencing or drug treatment applied to test KapB-mediated
158 PB disassembly. We also observed that mDia1 silencing did not eliminate SF formation (Fig 1D)
159 but, instead, increased elongated cells with visible actin SFs across the cell in both vector and
160 KapB conditions. The visible actin structures may represent different SF subtypes or actin
161 bundles that compensate for the loss of mDia1 (Hotulainen and Lappalainen 2006).
162 ROCK promotes SF formation by increasing actin contractility and inhibiting actin severing
163 activity (Julian and Olson 2014). Chemical inhibition of both isoforms of ROCK, ROCK1 and
164 ROCK2, with Y-27632 (Ishizaki et al. 2000) restored PBs in KapB-expressing cells and
165 increased the ratio of KapB:Vector PBs (Fig 2A-C). HUVECs treated with Y-27632 had
166 scalloped cell edges with minimal actin structure (Fig 2A). Y-27632 did not visibly alter cell
167 viability during the indicated treatment. To determine whether PB disassembly is dependent on a
168 single ROCK isoform, both ROCK1 and ROCK2 were knocked down with isoform-specific
169 shRNAs. Knockdown efficacy was confirmed with immunoblotting (Fig S1). Independent
170 knockdown of ROCK1 and 2 increased PBs counts in KapB-expressing cells (Fig 2D, F) and
171 restored the ratio of KapB:Vector PBs counts (Fig 2E). This indicated that both ROCK1 and
172 ROCK2 can contribute to KapB-mediated PB disassembly. ROCK2 knockdown showed more
173 robust PB restoration, both in terms of PB counts and PB size, than that seen with ROCK1
174 knockdown (Fig 2D, F). Quantification of PB counts in control cells for both pan-ROCK
175 inhibition and ROCK knockdown experiments is reported in Figure S1. While pan-ROCK
176 inhibition and ROCK1 knockdown treatments both eliminate SFs, ROCK2 knockdown retains
177 pronounced actin fibres in the cells (Fig 2F). Similar to mDia1 knockdown, this may indicate a
178 compensatory mechanism to retain cell shape and suggests that only a subset of SFs may be
179 required for PB disassembly. Taken together, these data show that inhibition of RhoA effectors
180 that mediate SF formation can reverse KapB-mediated PB disassembly. Put another way, we

181 have been unable to uncouple KapB-mediated SF formation from KapB-mediated PB
182 disassembly.
183 ROCK phosphorylates and activates LimK, which then phosphorylates and inactivates
184 cofilin, an actin-severing protein (Ohashi et al. 2000). In this way, ROCK promotes SF formation
185 by inactivating cofilin. To investigate the role of cofilin in KapB-mediated PB disassembly,
186 shRNAs to knockdown cofilin expression were used (Fig S2). Since ROCK activation results in
187 less cofilin activity and reduced actin severing, we hypothesized that knockdown of cofilin in
188 KapB-expressing cells would augment KapB-mediated PB disassembly. Knockdown of cofilin
189 resulted in elongated cells with more SFs in both control and KapB-expressing cells (Fig S2).
190 Cofilin knockdown also induced PB disassembly in control cells and aided PBs disassembly in
191 KapB-expressing cells (Fig S2 B, C). This indicates that inhibition of cofilin elicits PB
192 disassembly and supports the hypothesis that reducing cofilin activity is one of the reasons that
193 KapB promotes SF formation and PB disassembly.
194
195 **G-actin concentration does not influence PB disassembly**
196 Since we could not uncouple the signalling controlling SF formation from PB
197 disassembly, we investigated whether changes in the concentration of monomeric G-actin,
198 known to control cellular stress and SRF transcriptional responses (Sotiropoulos et al. 1999;
199 Chambers et al. 2015), could be controlling PBs. Several studies have shown that increasing the
200 proportion of filamentous actin decreases the cytoplasmic concentration of monomeric G-actin
201 (Rasmussen et al. 2010; Bunnell et al. 2011; Chambers et al. 2015). We investigated if our
202 phenotype, PB disassembly, was controlled by changes in the proportion of monomeric G-actin.
203 To determine this, cells were treated with drugs known to either decrease or increase the
204 proportion of monomeric G-actin. Jasplakinolide (Jasp) treatment decreases the G-actin fraction
205 by facilitating actin nucleation and aberrant polymerization of actin (Bubb et al. 1999).
206 Conversely, the actin polymerization inhibitor Cytochalasin D (CytD) caps the barbed end of
207 actin filaments, preventing further elongation of the actin filament and increasing the free G-
208 actin concentration (Wakatsuki et al. 2001). Jasp treatment, which prevents imaging of actin
209 structure due to interference with phalloidin (Fig S3C) (Bubb et al. 1999), resulted in an
210 increased F-actin fraction in HUVECs (Fig S3D). CytD treatment resulted in HUVECs with little
211 to no filamentous actin structure (Fig S3C). If the level of G-actin is the signal that regulates PB

212 dynamics, we hypothesized that Jasp, which decreases G-actin levels, would mediate PB
213 disassembly, while CytD would do the opposite, and promote PB assembly. However, both
214 treatments increased the PB count per cell (Fig S3A-C); these data indicate that the concentration
215 of G-actin does not influence PB disassembly, and this is not the mechanism by which actin SF
216 formation or enhanced activity of RhoA alters PB dynamics. These data are congruent with our
217 mDia1 and ROCK knockdown experiments that show retention of visible F-actin bundles despite
218 PB restoration.
219
220 **α −actinin-1 activity promotes PB disassembly**
221 The actinins are primarily known for their role in bundling actin fibres, though in non-
222 muscle cells, α -actinin-1 and 4 do not mediate actin bundling to the same extent (Pellegrin and
223 Mellor 2007). α -actinin-4 can, at times, localize to dorsal SFs, but it primarily mediates focal
224 adhesion turnover and can act as a transcriptional regulator of genes associated with cell
225 proliferation and differentiation (Honda et al. 1998; Kovac 2010; Honda 2015). α -actinin-1
226 primarily mediates SF bundling and formation, as well as focal adhesion maturation (Honda et
227 al. 1998; Kovac 2010). Using immunofluorescence, we observed that the localization of the two
228 isoforms seen in HUVECs (Fig S4A, B) was consistent with the reported localization and
229 function, as α -actinin-1 was localized to actin fibres and α -actinin-4 was more diffusely
230 cytoplasmic and nuclear, with some actin fibre localization (Honda et al. 1998; Kovac 2010).
231 Since α-actinin-1 associated with SFs in HUVECs and overexpression of α-actinin-GFP has
232 been shown to localize and reinforce SFs (Edlund, Lotano, and Otey 2001; Jackson et al. 2008),
233 we asked whether its overexpression would promote PB disassembly. Overexpression of
234 ACTN1-GFP resulted in elongated ECs with large SFs (Fig S4C). ACTN1-GFP decreased EDC4
235 puncta per cell, suggesting that enhancing SF bundling and focal adhesion maturation positively
236 regulates PB disassembly (Fig S4C, D).
237
238 **Changes in cytoskeletal contractility control PB disassembly**
239 One of the downstream activities of the kinase, ROCK, is to phosphorylate myosin light
240 chain to induce non-muscle myosin II (NMII)-mediated actomyosin contraction (Mutsuki
241 Amano et al. 1996). Since ROCK is required for KapB-mediated PB disassembly, we
242 determined whether functional actomyosin contractility is also required. KapB-expressing cells

243 were treated with blebbistatin, which inhibits NMII-mediated actomyosin contractility by
244 maintaining NMII in a conformation that is unable to bind actin filaments (Kovacs et al. 2004).
245 Treatment of KapB-expressing cells with blebbistatin restored both PBs levels in KapB-
246 expressing cells, as well as the KapB:Vector ratio of PBs (Fig 3A-C), indicating that
247 contractility is required for KapB-induced PB disassembly. ECs treated with blebbistatin had
248 normal actin structure (Fig 3C). Blebbistatin treatment for the indicated time did not visibly
249 alter cell viability. To determine if contraction would elicit the same phenotype in the absence
250 of KapB, cells were treated with Calyculin A (CalA), an inhibitor of myosin light chain
251 phosphatase that promotes NMII phosphorylation and actomyosin contraction (Asano and
252 Mabuchi 2001). CalA treatment did not visibly alter actin cytoskeletal structure or cell viability.
253 Inducing contraction with CalA decreased counts of PBs (Fig 3D, E), again consistent with the
254 hypothesis that actomyosin contractility controls PB disassembly.
255 Actomyosin contractility impacts cytoskeletal tension in adherent cells with SFs (Katoh
256 et al. 1998; Tan et al. 2003). Additionally, both Jasp and CytD interfere with cytoskeletal
257 tension (Rotsch and Radmacher 2000), and both increased PB counts (Fig S3). Since the
258 mechanoresponsive transcription activator, YAP, is activated by increases to cytoskeletal
259 tension via actomyosin contractility (Dupont et al. 2011), we explored the role of YAP in KapB-
260 mediated PB disassembly.
261
262 **YAP is required for KapB-mediated PB disassembly**
263 To determine if YAP was involved in KapB-mediated PB disassembly, we expressed
264 shRNAs targeting YAP in KapB-expressing HUVECs to assess whether the altered levels of
265 YAP impacted PB disassembly. Immunoblotting confirmed knockdown efficiency of YAP (Fig
266 4A). Knockdown of YAP resulted in elongated HUVECs with mostly cortical actin fibres (Fig
267 4D). These cells displayed increased PBs in KapB-expressing cells (Fig 4B-D). In the context of
268 YAP knockdown, the KapB:Vector ratio of PBs counts was restored, indicating that YAP is
269 required for KapB-mediated PB disassembly (Fig 4C) and suggesting that KapB is activating a
270 mechanoresponsive signalling axis to elicit PB disassembly via YAP.
271 We next investigated the steady-state protein level and localization of YAP in KapB-
272 expressing cells. KapB-transduced HUVECs showed increased levels of nuclear YAP and total
273 YAP in some experiments, though the ratio of nuclear:cytoplasmic YAP was not markedly

274 increased (Fig S5A-B). When YAP is phosphorylated by LATS, it is sequestered in the
275 cytoplasm and transcriptionally inactive (Zhao et al. 2007). While YAP has multiple
276 phosphorylation sites, phosphorylation at serine 127 is the most potent LATS-mediated
277 phosphorylation site that promotes cytoplasmic distribution of YAP (Zhao et al. 2007). To
278 investigate the phosphorylation status of YAP in KapB-expressing cells, levels of P(S127)-YAP
279 and total YAP were measured by immunoblot. In KapB-expressing cells, there was a decrease in
280 the ratio of P(S127)-YAP to total YAP that may suggest YAP is more active when KapB is
281 expressed (Fig S5B). In some experiments, we observed an increase in total steady-state levels of
282 YAP by immunoblotting, corroborating the small increase in total YAP intensity seen by
283 microscopy (Fig S5A-B). Although increases in total YAP may suggest that YAP turnover is
284 blocked or decreased by KapB, these increases are not accompanied with the expected strong
285 decrease in phosphorylated YAP or an increase in percent of total YAP found in the nucleus, as
286 in (Pavel et al. 2018).
287 We next asked if active YAP can interact with TEAD and other transcription factors to
288 elicit changes in gene expression in KapB-expressing cells (Vassilev et al. 2001). We used a
289 TEAD-element luciferase assay to assess if canonical YAP transcription was activated. As a
290 positive control, we used YAP 5SA, a version of YAP that is unable to be phosphorylated and
291 inactivated by the inhibitory kinase LATS (Zhao et al. 2007) and is thus considered
292 constitutively active. YAP 5SA robustly activated the TEAD element-containing firefly
293 luciferase reporter (Fig S5C). KapB did not induce the transcription of the TEAD element-
294 containing firefly luciferase reporter (TEAD-Fluc; Fig S5C). Further, KapB did not increase
295 steady-state mRNA levels of common YAP target genes CTGF, CYR61 and ANKRD1 by RT-
296 qPCR, although these genes were elevated by YAP 5SA (Fig S5D). These data indicate despite
297 the observation that YAP may be more abundant in KapB-expressing cells, canonical YAP
298 targets are not upregulated.
299 We wondered if YAP activation could elicit PB disassembly in the absence of KapB
300 expression. To this end, we transduced HUVECs with YAP 5SA. YAP 5SA-expressing cells
301 contained few, thick actin fibres (Fig 5A) and displayed decreased number of PBs per cell,
302 indicating that YAP 5SA elicited disassembly of PBs (Fig 5A, B). We also confirmed that we
303 could stain PBs in control cells with antibodies for more than one PB resident protein (EDC4,
304 Dcp1a and DDX6) and that when YAP 5SA was expressed, loss of PB puncta was observed for

305 each of these staining conditions (Fig 5 A-F). KapB-mediated PB disassembly correlates with
306 increases in stability and levels of ARE-mRNA (Corcoran, Johnston, and McCormick 2015;
307 McCormick and Ganem 2005). To examine whether YAP 5SA-mediated PB disassembly elicits
308 the same changes in ARE-mRNAs, we used a luciferase assay we previously established to
309 measure the luminescence of an ARE-containing firefly luciferase reporter (Corcoran,
310 Khaperskyy, and McCormick 2011). In this assay, as previously shown in Corcoran, Johnston,
311 and McCormick (2015), KapB increased level of firefly luminescence indicating enhanced
312 stability or translation of its RNA transcript (Fig 5C). However, despite also inducing
313 pronounced PB disassembly, YAP 5SA did not increase Fluc luminescence significantly more
314 than the control construct (Fig 5C). This points to a divergence of KapB and active YAP
315 outcome. Although PB disassembly is induced by the expression of both YAP 5SA and KapB,
316 active YAP increases the transcriptional activation of genes CTGF, CYR61 and ANKRD1 while
317 KapB does not; conversely, KapB enhances the stability of ARE-mRNAs while active YAP does
318 not.
319 We wondered if PB disassembly did not require YAP to transactivate transcription of its
320 canonical genes. To better understand this mechanism, we transduced HUVECs with another
321 YAP construct called YAP 6SA (Fig 6). YAP 6SA contains the same mutations as 5SA; in
322 addition, it cannot be phosphorylated by AMPK at serine 94 (Mo et al. 2015). This
323 phosphorylation event is essential for its interaction with TEAD; therefore, the S94A mutation
324 renders YAP 6SA transcriptionally inactive (Mo et al. 2015, Zhang et al. 2017). We observed
325 that unlike YAP 5SA or KapB, YAP 6SA did not appear to elongate cells, suggesting that actin
326 dynamics were unaffected, as in Pavel et al. (2018). Compared to YAP 5SA which caused
327 pronounced PB disassembly, YAP 6SA failed to alter PB levels compared to vector controls (Fig
328 6B). This was confirmed by staining PBs with antibodies for two different resident proteins,
329 DDX6 and EDC4 (Fig 6A).
330
331 **YAP activators disassemble PBs**
332 Since overexpression of constitutively active YAP 5SA leads to disassembly of PBs, we
333 wanted to determine whether other stimuli that activated endogenous YAP could do the same.
334 We tested various upstream mechanical signals described to activate YAP for their ability to
335 elicit PB disassembly: shear stress, low cell confluence and high ECM stiffness (Nakajima et al.

336 2017; Lee et al. 2017; Noria et al. 2004; Zhao et al. 2007; Dupont et al. 2011). For the first, we
337 subjected HUVECs to shear stress by fluid flow (shear forces of 2 and 10 dyn/cm^2) and PBs were
338 examined via immunofluorescence using antibodies to both EDC4 and DDX6. Both treatments
339 showed prominent cell elongation, stress fibre formation, and resulted in robust PB disassembly
340 of both EDC4-positive and DDX6-positive puncta (Fig 7A, B). To test if cell confluence
341 regulates PB levels, HUVECs were seeded at low, medium and high densities. Cells at low
342 confluence are reported to have active YAP and we predicted PBs would disassemble; however,
343 the low-density monolayer displayed more PBs per cell then those at medium and high densities
344 (Fig 7C, D). To test the impact of collagen stiffness on PB disassembly, HUVECs were plated on
345 coverslips coated with increasing densities of collagen (0 to 64 μg/ cm^2). While collagen density
346 does not perfectly reproduce matrix stiffness as it does not differentiate the effect of matrix
347 stiffness from increasing collagen-binding sites, increasing collagen densities do correlate with
348 increased matrix stiffness (Yang, Leone, and Kaufman 2009; Lee et al. 2014; Joshi, Mahajan,
349 and Kothapalli 2018). As collagen density increased, PBs decreased (Fig 7E, F). Notably, as
350 collagen density increased, only slight increases in visible actin fibres were noted (Fig 7E),
351 suggesting the tested range of stiffness was small and should be expanded in future studies.
352 Taken together, these data indicate that PB disassembly occurred in response to mechanical
353 stimuli known to require RhoA and altered cytoskeletal structures to activate YAP (shear stress
354 and increased ECM concentration) (Zhao et al. 2012; Huang et al. 2016; Lee and Kumar 2016;
355 Moreno-Vicente et al. 2018). Again, our model points to the importance of actin SF formation as
356 a requisite precursor to PB disassembly irrespective of YAP activation status.
357
358 **Shear stress mediated PB disassembly requires YAP**
359 YAP responds to external forces that induce active RhoA, actin SFs, and pronounced cell
360 elongation; in short, the typical behaviour of ECs in response to the mechanical shear stress that
361 is produced by fluid flow. However, how YAP responds to shear stress is controversial (Wang et
362 al. 2016; Huang et al. 2016; Lee et al. 2017; Nakajima and Mochizuki 2017). To verify YAP
363 activation by continuous, unidirectional fluid flow in our system, HUVECs subjected to 2 and 10
364 dyn/cm^2 of shear stress were lysed and used for immunoblotting for P(S127)-YAP and total
365 YAP. Shear stress decreased the ratio of phospho-YAP/YAP in both conditions, suggesting a
366 higher proportion of active YAP (Fig 8A). To assess if YAP was required for PB disassembly in

367 response to shear stress, HUVECs transduced with YAP-targeting shRNA were subjected to 10
368 dyn/cm^2 shear stress. PBs disassembled in cells treated with a non-targeting shRNA when
369 subjected to shear stress (Fig 8B, C), consistent with earlier experiments (Fig 7A, B). When YAP
370 was reduced by shRNA expression, ECs exposed to shear stress had more PBs than static growth
371 control cells (Fig 8B, C). YAP knockdown also reduced the cells ability to form SFs, with many
372 cells displaying highly cortical phalloidin staining and fewer actin fibres across the cell (Fig 8C).
373 Therefore, YAP is required to disassemble PBs after KapB is expressed and also in response to
374 shear stress.

375 Recently, an important connection has emerged between YAP and autophagy. Active
376 YAP was previously shown to upregulate the transcription of Armus, a Rab7-GTPase activating
377 protein required for autophagosome fusion with the lysosome, the final step in the autophagic
378 pathway (Totaro et al. 2019, Carroll et al. 2013). Moreover, stimuli that promote active YAP
379 activate autophagic flux by inducing the transcription of TEAD-responsive genes that regulate
380 actomyosin, including ACTNB and MYOII (Pavel et al. 2018). These data showed that actin and
381 myosin modulate the trafficking of key autophagy proteins (such as Atg16L1 and Atg9A) that
382 are required for autophagosome formation and that this process is a downstream effect of YAP
383 activation and YAP 5SA (Pavel et al. 2018).

384 To examine the connection between YAP and autophagic flux as it pertains to PB
385 disassembly, we used immunofluorescence to stain for the autophagy marker, LC3, which forms
386 puncta that represent autophagosomes (Fig S6). YAP5SA-expressing cells did not have more
387 LC3 puncta than vector controls, and LC3 puncta did not increase after treatment with
388 Bafilomycin A1 (an inhibitor of lysosomal acidification and autophagosome-lysosome fusion,
389 Mauvezin and Neufeld, 2015) (Fig S6C). The lack of LC3 puncta increase in YAP 5SA-
390 expressing cells after Bafilomycin A1 treatment could mean that autophagy is not increased. It
391 could also mean that autophagic flux and degradation are both increased, LC3 is degraded
392 rapidly and LC3 puncta fail to accumulate. The latter interpretation is most consistent with
393 previous reports which showed that YAP 5SA enhances autophagic flux (Pavel et al. 2018) and
394 promotes autophagosome-lysosome fusion (Totaro et al 2019). We also observed that YAP 5SA
395 increased the transcription of Armus, involved in activation of Rab7 for autophagosome-
396 lysosome fusion, while KapB did not (Fig S6E). To determine if enhanced autophagic flux and
397 accelerated autophagosome turnover caused by YAP 5SA contributes to PB disassembly, we

398 treated YAP 5SA-expressing cells with Bafilomycin A1 to block the final autophagy step, and
399 stained for PBs (Fig S6C, D). We observed that Bafilomycin A1 did not restore PBs in YAP
400 5SA-expressing cells (Fig S6C, D). This suggests the possibility that autophagy is not the
401 primary mechanism required for PB disassembly induced by YAP 5SA, and that other inputs or
402 factors are also involved.
403 Taken together with our analysis of KapB-mediated PB disassembly, these data suggest
404 that when KapB is expressed, it turns on mechanoresponsive signals that endothelial cells use to
405 withstand mechanical forces like shear, in the absence of an external stimulus. The outcome of
406 both scenarios is YAP-dependent disassembly of cytoplasmic PBs.
407
408 **Discussion**
409 In this manuscript, we have used a viral protein from an oncogenic virus to uncover the
410 relationship between cytoplasmic PBs and the mechanical regulation of actin SF formation. We
411 present data to support the existence of a mechanoresponsive pathway that links actin SFs,
412 actomyosin contractility, and the transcription transactivator YAP to the disassembly of PBs and
413 show that this pathway is hijacked by KapB during KSHV latency. Our major findings are as
414 follows. i) KapB-mediated PB disassembly requires actin SF effectors ROCK1/2 /mDia1 and is
415 enhanced by loss of the actin-severing protein, cofilin. ii) KapB-mediated PB disassembly is
416 reversed when blebbistatin is used to inhibit actomyosin contractility or after knockdown of the
417 mechanoresponsive transcription transactivator, YAP. iii) In the absence of KapB, we can induce
418 PB disassembly when we promote the formation of actin SFs, actomyosin contractility, and YAP
419 activity using overexpression of α−actinin-1 (promotes actin bundling into SFs and increases
420 cytoskeletal tension (Jackson et al. 2008)), Calyculin A (inhibits myosin light chain phosphatase
421 to promote actomyosin contraction (Asano and Mabuchi 2001)), or overexpression of active
422 YAP (YAP 5SA). Exposure of endothelial cells to the external forces created by shear stress or a
423 stiff extracellular matrix also induces PB disassembly in the absence of KapB. iv)
424 Overexpression of transcriptionally inactive YAP (YAP 6SA) fails to disassemble PBs,
425 indicating that YAP's role as a transcription transactivator is important for its ability to promote
426 PB disassembly. Together, these data show for the first time, that PBs disassemble in response to
427 mechanical signals that transduce external forces from outside the cell to the actin cytoskeleton
428 and that this is a pathway used by endothelial cells to regulate gene expression in response to

429 diverse stimuli. Moreover, this work also highlights the remarkable pizzazz used by viruses to
430 hijack cellular pathways. In this case, we reveal that the viral protein KapB taps into this
431 mechanoresponsive pathway to trigger mechanical changes to cytoskeletal structures and
432 downstream effectors that would normally respond to force, thereby inducing PB disassembly
433 from within the cell, rather than from without.

434 During the process of actin polymerization, the monomeric form of actin, globular actin
435 (G-actin), aggregates in groups of three subunits or more to nucleate an actin filament, which
436 extends into filaments via addition of further G-actin monomers through ATP-dependent
437 polymerization (reviewed in Pollard 2016). 10 to 30 actin filaments (F-actin) bundle together
438 into SFs, primarily using the α-actinin family for crosslinking (Small et al. 1998; Cramer,
439 Siebert, and Mitchison 1997; Lazarides and Burridge 1975; Pellegrin and Mellor 2007). SFs with
440 periodic distribution of actin-crosslinking proteins and non-muscle myosin II (NMII) are
441 contractile structures (Katoh et al. 1998; Tan et al. 2003), but not all actin SFs function equally in
442 this regard. For any structure to be able to generate tension, it must be tethered at the ends. Of the
443 types of SFs (ventral SFs, dorsal SFs and transverse arcs; (Small et al. 1998)), ventral SFs are
444 attached at both termini to the extracellular matrix (ECM) through focal adhesions and contain
445 NMII, which imparts a contractile phenotype (Hotulainen and Lappalainen 2006; Small et al.
446 1998; Vallenius 2013). Dorsal SFs are attached through focal adhesions but do not contain NMII,
447 and thus are not contractile (Small et al. 1998; Vallenius 2013). However, dorsal SFs are thought
448 to work in concert with transverse arcs, which contain NMII but are not attached to focal
449 adhesions, to mediate cellular contractility.

450 Several features of our data suggest that the structures that are important for KapB-
451 mediated PB disassembly must be contractile and cause cytoskeletal tension. When both mDia1
452 and ROCK2 were silenced in KapB-expressing cells (Fig 1, 2), visible actin bundles are still
453 apparent despite PB restoration in both contexts. This suggests that not all SF subtypes are
454 required for our phenotype. In addition, blebbistatin treatment of KapB-expressing cells
455 dramatically restored PBs; these data suggest that PB disassembly requires actin-mediated
456 contractility rather than merely structural support (Fig 3). Furthermore, overexpression of α-
457 actinin and shear stress increase cell stiffness (Lee et al. 2006; Jackson et al. 2008) and both
458 treatments induced PB disassembly (Fig S4, Fig 7), reinforcing the correlation between
459 increasing cell tension and PB disassembly. Finally, our data show that YAP is required for PB

460 disassembly (Figs 4, 5, 8). YAP is mechanoresponsive; it becomes active when tension-forming
461 actin structures are induced by external forces e.g. focal adhesion engagement by stiff ECM
462 (Dupont et al. 2011; Sugimoto et al. 2018). As YAP activation and PB disassembly both rely on
463 RhoA-induced cytoskeletal contractility, any activator of YAP that induces cytoskeletal tension
464 through RhoA should mediate PB disassembly. Our data supports this notion, as shear stress
465 forces and increasing collagen density both cause PB disassembly in the absence of KapB, while
466 low confluence does not (Fig 7). We also know that GPCRs ($G_{11/12}$ and $G_{q/}$11) activate YAP in a
467 RhoA-dependent manner (Yu et al. 2012) and LPA treatment or overexpression of KSHV-
468 derived constitutively active vGPCR (both activate $G_{11/12}$) both induce PB disassembly (Corcoran
469 et al. 2012; Corcoran and McCormick 2015). These findings support the conclusion that PB
470 disassembly requires the formation of contractile actin structures like those associated with YAP
471 transactivation responses.
472 KSHV is an oncogenic virus associated with the endothelial neoplasm, Kaposi's sarcoma
473 (KS). Cells within the KS lesion display latent KSHV infection, proliferate abnormally, spindle,
474 and release many pro-inflammatory and pro-tumourigenic mediators into the microenvironment.
475 KapB expression alone recapitulates two of these key features, cell spindling and pro-
476 inflammatory mediator production that results from enhanced stability of ARE-containing
477 cytokine mRNAs that would normally shuttle to PBs for constitutive turnover (Corcoran,
478 Johnston, and McCormick 2015). Our previous work showed that both phenotypes utilize KapB
479 activation of the stress-responsive kinase, MK2, and the downstream activation of the GTPase
480 RhoA (Corcoran, Johnston, and McCormick 2015; Corcoran and McCormick 2015). We also
481 showed that the lytic vGPCR protein mediates PB disassembly and the concomitant stabilization
482 of ARE-mRNAs, while more recently ORF57 has been also reported to disrupt PBs (Corcoran et
483 al. 2012; Sharma et al. 2019). The observation that KSHV encodes at least three separate gene
484 products sufficient to drive PB disassembly suggests that PB disassembly is beneficial for some
485 aspect of the infectious cycle. Further research is required to definitively address how PBs
486 influence the KSHV infectious cycle and the fate of infected cells.
487 We and others observed that the presence or absence of PB punctae visible by
488 microscopy directly correlates with the stability of ARE-mRNAs (Corcoran, Johnston, and
489 McCormick 2015; Vindry et al. 2017; Blanco et al. 2014). We predicted that YAP- mediated PB
490 disassembly would also promote ARE-mRNA stability. Indeed, several YAP-target genes

491 contain ARE elements in their 3'UTR, including CTGF and ANKRD1 (Shen and Stanger 2015;
492 Bakheet, Hitti, and Khabar 2017). Shear forces also cause YAP-dependent PB disassembly and
493 have previously been shown to upregulate many genes containing ARE-mRNAs (Vozzi et al.
494 2018; Bakheet, Hitti, and Khabar 2017). However, in our studies overexpression of constitutively
495 active YAP (YAP 5SA) disassembled PBs but did not increase stability of an ARE-containing
496 firefly luciferase reporter (Fig 5) (Corcoran, Khaperskyy, and McCormick 2011)). This may be
497 due to different functional responses for different classes of AU-rich elements. Our ARE-
498 containing luciferase reporter contains the AU-rich sequence derived from the 3'-UTR of GM-
499 CSF, categorized in Cluster 5, whereas canonical YAP genes CTGF and ANKDR1 are in
500 Clusters 1 and 2, respectively (Bakheet, Hitti, and Khabar 2017). This discrepancy may also
501 result from the dual function of PBs as sites of translational suppression as well as RNA decay,
502 supported by observations that PBs decreases do not always correlate with decreased mRNA
503 turnover (Eulalio, Behm-Ansmant, and Izaurralde 2007, Horvathova et al. 2017, Tutucci et al.
504 2018, Wilbertz et al. 2019, Hubstenberger et al. 2017).
505 Data presented herein clearly implicate a requirement for YAP in the PB disassembly
506 phenotype that is induced by KapB and by the external force, shear stress (Fig 4, 8). However,
507 the precise connection between YAP and PB disassembly is unclear. What we do know is that
508 despite the clear reliance on YAP for PB disassembly, KapB does not increase expression of
509 canonical YAP-regulated transcripts (Fig S5). Our data also show small increases in total YAP
510 and small decreases in the ratio of phosphorylated/total YAP; however, the ratio of
511 nuclear:cytoplasmic YAP is not markedly altered (FigS5). Taken together, these data suggested a
512 model whereby PB disassembly was independent of YAP's role as a gene transactivator and
513 YAP nuclear translocation. However, we found that overexpression of YAP 6SA, which is
514 unable to act as a transcription transactivator, fails to cause PB disassembly (Fig 6), indicating
515 that this transcription induction function of YAP is required for its role in regulating PB
516 dynamics. In the discussion that follows, we describe our working model (Fig 9) for how YAP
517 may promote PB disassembly.
518 *MODEL: YAP promotes autophagy to cause PB disassembly* (Fig 9). Several studies link
519 YAP with the regulation of the catabolic process of autophagy, though many of these are
520 contradictory and suggest YAP-mediated autophagy control is cell type and context-dependent
521 (Song et al. 2015; Liu et al. 2017; Pei et al. 2019; Totaro et al. 2019, Pavel et al 2018). Totaro et

522 al. provided evidence that YAP promotes autophagic catabolism by promoting the expression of
523 Armus, a Rab7-GTPase activating protein that is required to mediate the fusion of
524 autophagosomes with lysosomes in the final degradative step of autophagy (Totaro et al. 2019).
525 In addition, stimuli that activate YAP promote autophagic flux by inducing the transcription of
526 TEAD-responsive genes that regulate actomyosin, including ACTNB and MYOII (Pavel et al.
527 2018). These data showed that actin and myosin modulate the trafficking of key autophagy
528 proteins (such as Atg16L1 and Atg9A) that are required for autophagosome formation and that
529 this process is a downstream effect of YAP activation (Pavel et al. 2018). These data also show
530 that YAP 5SA promotes autophagic flux while YAP 6SA does not, consistent with YAP-
531 dependent autophagy upregulation requiring YAP transcriptional responses. This emerging
532 connection between YAP and autophagy suggests that the latter is a mechanoresponsive process;
533 this is also supported by other studies wherein endothelium exposed to unidirectional shear stress
534 upregulates autophagy (Liu et al. 2015; Yao et al. 2015; Wang et al. 2018; Das et al. 2018, Hardy
535 et al. 2017). These data are also consistent with new data from our group showing that PB
536 disassembly mediated by KapB requires autophagy, as knockdown of a canonical autophagy
537 gene (Atg5) or treatment with Bafilomycin A1 restored PBs (Robinson et al. 2021). However,
538 YAP 5SA-mediated PB disassembly was not restored by Bafilomycin A1 treatment (Fig 5 -
539 Figure Supplement 1). This difference may be due, in part, to the higher levels of Armus
540 expression in YAP 5SA-expressing cells compared to KapB-expressing cells (Fig S6). This
541 would imply that although both YAP 5SA and KapB enhance autophagic flux, only YAP 5SA
542 also accelerates the final degradative step of autophagy (Fig 9).
543 PBs are sites where innate immune factors congregate that are disrupted by most viruses
544 during infection (Burdick et al. 2010; Li et al. 2012; Ostareck, Naarmann-de Vries, and
545 Ostareck-Lederer 2014; Burgess and Mohr 2015; Cuevas et al. 2016; H. Wang et al. 2016; Lumb
546 et al. 2017; Balinsky et al. 2017; Núñez et al. 2018; Ng et al. 2020). Indeed, KSHV encodes three
547 separate proteins that all induce PB disassembly, suggesting this event is central to viral
548 persistence (Corcoran et al. 2012; Corcoran, Johnston, and McCormick 2015; Sharma et al.
549 2019). PBs are likely playing an as yet undefined and underappreciated role in regulating innate
550 antiviral responses. YAP is also an unappreciated negative regulator of innate immune signaling
551 pathways. YAP blocks the ability of the innate immune kinase, TBK1, a downstream effector for
552 several innate signaling pathways, to associate and activate its substrates (Zhang et al 2017). In

553 so doing, YAP blocks downstream induction of interferons and increases viral replication (Zhang
554 et al. 2017). However, this feature of YAP is independent of its ability to act as a transcriptional
555 transactivator (Zhang et al. 2017). Based on our data that show YAP 5SA causes PB disassembly
556 while YAP 6SA does not, we think it most likely that KapB-induced PB disassembly requires the
557 transcription transactivation function of YAP. We also speculate that KapB-induced PB
558 disassembly, like active YAP, favours viral replication and survival and is promoted by KSHV in
559 order to reshape subsequent antiviral innate immune responses.
560 In this manuscript, we describe the surprising convergence of two previously unrelated
561 yet essential regulators of cellular gene expression – the mechanoresponsive transactivator YAP
562 and cytoplasmic PBs, known sites of AU-rich cytokine mRNA decay. We show that PB
563 disassembly is mechanoresponsive; external forces that change cell shape and tension-forming
564 cytoskeletal structures cause PB disassembly in a YAP-dependent manner. This discovery was
565 made courtesy of the unique KSHV protein, KapB, and provides yet another example of how
566 viruses have evolved surprising ways to manipulate their host and ensure their survival. In this
567 case, KapB induces, from the inside out, a mechanoresponsive pathway to cause PB
568 disassembly. Future study will untangle how these related mechanoresponsive events are induced
569 by KSHV to better promote viral replication.
570
571

572 **Materials and Methods**

573 **Antibodies, Plasmids and Reagents**

574 The antibodies used in this study can be found in Table S1. The plasmids used in this
575 study can be found in Table S2. Forward and reverse shRNA sequences were selected from the
576 TRC Library Database in the Broad Institute RNAi consortium. YAP target shRNAs in pLKO.1
577 were obtained from Dr. C. McCormick (Dalhousie University, Halifax, Canada). Sequences for
578 all shRNA oligonucleotides used for cloning are listed in Table S3. Cloning of shRNAs was
579 conducted according to the pLKO.1 protocol (Addgene 2006). YAP 6SA was subcloned into
580 pLJM1 by PCR amplification using primers (For: 5'-CGTAACCGGTATGGATCCCGGGCA-
581 3', Rev: 5'-CTGATAAGTCGACAACCACTTTGTACAAGAAAGTTG-3') designed to remove
582 the V5 tag and insert a stop codon as well as 5' AgeI and 3' SalI restriction enzyme sites. The
583 chemical inhibitors used in this study can be found in Table S4.

584 **Cell Culture**

585 Human embryonic kidney 293T and 293A cells (HEK-293T/A, ATCC, Manassas,
586 Virginia, US) and human cervical adenocarcinoma cells expressing a tetracycline-inducible
587 repressor (HeLa Tet-Off, Clontech, Mountain View, California, US) were cultured in Dulbecco's
588 Modified Eagle Medium (DMEM, Gibco, Carlsbad, California, US) supplemented with 10%
589 heat-inactivated fetal bovine serum (Gibco), 100 U/mL penicillin, 100 μg/mL streptomycin, and
590 2 mM L-glutamine (Gibco). Pooled human umbilical vein endothelial cells (HUVECs, Lonza,
591 Basel, Switzerland) were cultured in endothelial cell growth medium 2 (EGM-2, Lonza)). For
592 HUVEC passaging, tissue culture plates were precoated for 30 min at 37°C with 0.1% (w/v)
593 porcine gelatin (Sigma, St. Louis, Missouri, US) in 1X PBS (Gibco). All cells were routinely
594 tested for mycoplasma by PCR method.

595 **Transfection for Lentivirus Production**

596 HEK-293T cells at 70-80% confluence were transfected using 3.3 μg of the target
597 lentiviral construct, 2 μg pSPAX2 and 1 μg pMD2.G with 1 mg/mL polyethyenimine (PEI,
598 Sigma) in serum-free DMEM. After 5 to 6 h, media was replaced with antibiotic-free DMEM
599 containing 10% FBS and 2 mM L-glutamine (Gibco). Transfected cells were incubated for 48 h
600 at 37°C to allow lentivirus production. The supernatant media containing viral particles was
601 harvested and filtered through a 0.45 μm polyethersulfone (PES) filter (VWR, Randor,
602 Pennsylvania, US) and aliquoted. Virus was stored at -80°C until use.

603 **Lentiviral Transduction**

604 Lentivirus was supplied into wells of plated HUVECs in EGM-2 supplemented with 5
605 μg/mL hexadimethrine bromide (polybrene). After 24 h incubation, cells were selected with
606 either 5 μg/mL blasticidin (Sigma) for 96 h, replacing the media and antibiotic at 48 h, or 1
607 μg/mL puromycin (Sigma) for 48 h. Following selection, HUVEC medium was replaced with
608 EGM-2 without selection for at least 24 h recovery before further use. Lentivirus was titrated to
609 ensure no significant changes in cell viability from non-targeting control.

610 **Immunofluorescence**

611 Immunofluorescence was performed as described previously (Corcoran, Johnston, and
612 McCormick 2015). Briefly, cells were grown on coverslips (no. 1.5, Electron Microscopy
613 Sciences, Hatfield, Pennsylvania, US). Following treatment, coverslips were fixed in 4%
614 paraformaldehyde (PFA, Electron Microscopy Sciences) in PBS at 37°C for 10 min,
615 permeabilized with 0.1% Triton-X100 (Sigma) in 1X PBS for 10 min at RT, and blocked in 1%
616 Human AB serum (blocking buffer, Sigma) in 1X PBS for 1 h at RT. An exception to this is
617 samples being prepared for staining endogenous LC3, which were fixed and permeabilized in
618 ice-cold methanol prior to blocking. Coverslips were then incubated with diluted primary
619 antibody in blocking buffer overnight at 4°C in a humidified chamber. After primary antibody
620 incubation, coverslips were washed with 1X PBS and then incubated in fluorescently-tagged
621 secondary antibody diluted in blocking buffer for 1 h at RT. If applicable, coverslips were
622 stained with Phalloidin-conjugated Alexa-Fluor 647 (Invitrogen, 1:100) in 1X PBS for 1.5 h.
623 Coverslips were mounted onto microscope slides (FisherBrand, Pittsburgh, Pennsylvania, US)
624 using Prolong Gold Antifade Mounting Media (Invitrogen, Carlsbad, California, US). For
625 coverslips that were used for EDC4 puncta quantification, the following modifications to
626 immunofluorescence were made: (1) Prior to permeabilization, coverslips were stained with
627 wheat germ agglutinin (WGA) Alexa-647 conjugate (Invitrogen, 1:400) in 1X PBS for 10 min at
628 RT. (2) Following secondary antibody incubation, coverslips were stained with 4',6-Diamidino-
629 2-Phenylindole (DAPI, Invitrogen, 1:10,000) in 1X PBS for 5 min.

630 Confocal imaging was performed on the Zeiss LSM 880 Confocal Microscope
631 (Charbonneau Microscopy Facility, University of Calgary, Calgary, Canada) at the 63X oil
632 objective. CellProfiler imaging was performed on the Zeiss AxioImager Z2 (CORES facility,

633 Dalhousie University, Halifax, Canada) or Zeiss AxioObserver (Charbonneau Microscopy
634 Facility, University of Calgary) at the 40X oil objective.

635 **Quantification of Processing Bodies Using CellProfiler Analysis**

636 CellProfiler (cellprofiler.org) is an open source software for high-content image analysis
637 (Kamentsky et al. 2011) and was used to develop an unbiased method for quantifying changes to
638 PB dynamics. The pipeline used for quantifying PBs was structured as follows: To detect nuclei,
639 the DAPI image was thresholded into a binary image. In the binary image, primary objects
640 between 30 to 200 pixels in diameter were detected and defined as nuclei. Cells were identified
641 as secondary objects in the WGA image using a propagation function from the identified nuclei,
642 which determined the cell's outer edge. Using the parameters of a defined nucleus and cell
643 border, the cytoplasm was then defined as a tertiary object. The EDC4 channel image was
644 enhanced using an "Enhance Speckles" function to identify distinct puncta and eliminate
645 background staining. The cytoplasm image was then applied as a mask to the enhanced puncta
646 image to ensure quantitation of only cytoplasmic puncta. EDC4 puncta were measured in the
647 cytoplasm of cells using a 'global thresholding with robust background adjustments' function as
648 defined by the program. The threshold cut-off for identified EDC4 puncta remained constant
649 between all experiments with identical staining parameters. Puncta number per cell, intensity and
650 locations with respect to the nucleus were measured and exported as .csv files and analyzed in
651 RStudio. A template of the RStudio analysis pipeline is attached in Appendix A. Data was
652 represented as fold change in EDC4 puncta count per cell normalized to the vector puncta count.
653 'Relative EDC4 Puncta/Cell (KapB/Vector)' demonstrates the KapB puncta count divided by
654 vector puncta count, a ratio that was calculated within each treatment group for each biological
655 replicate.
656

657 **Protein Electrophoresis and Immunoblotting**

658 Cells were lysed in 2X Laemmli buffer (20% glycerol, 4% SDS, 120 mM Tris-HCl),
659 between 150 to 300 μL, depending on cell density. Lysates were homogenized with a 0.21-gauge
660 needle, and supplemented to contain 0.02% (w/v) bromophenol blue (Sigma) and 0.05 M
661 dithiothreitol (DTT, Sigma), then heated at 95˚C for 5 min. 7.5 or 12% TGX Stain-Free SDS-
662 polyacrylamide gels (BioRad) were cast according to the instructions of the manufacturer and 5
663 to 15 μg of total protein were subjected to SDS gel electrophoresis using 1X SDS running buffer

664 (25 mM Tris, 192 mM Glycine, 0.1% SDS). Precision Plus Protein All Blue Prestained Protein
665 Standards (BioRad, Hercules, California, US) was used as a molecular weight marker. After
666 electrophoresis, gels were UV-activated using the ChemiDocTouch (BioRad) Stain-Free Gel
667 setting with automated exposure for 45 s. The protein was transferred to low-fluorescence
668 polyvinylidene difluoride (PVDF) membranes (BioRad) on the Trans-Blot Turbo Transfer
669 System (BioRad) according to the instructions of the manufacturer. Following transfer, total
670 protein amounts on membranes were imaged on the ChemiDocTouch using the Stain-Free
671 Membrane setting with automated exposure. Membranes were then blocked using 5% BSA
672 (Sigma) in 1X TBS-T (150 nM NaCl, 10 mM Tris, pH 7.8, 0.01% Tween-20) for 1 h at RT.
673 Primary antibody was diluted in 2.5% BSA in 1X TBS-T. Membranes were incubated in
674 primary antibody solution overnight at 4˚C with rocking. The following day, membranes were
675 washed 3 times for 5 min in 1X TBS-T. Membranes were incubated with the appropriate
676 secondary antibody, conjugated to horseradish peroxidase (HRP) for 1 h at RT. Membranes were
677 washed 4 times for 5 min in 1X TBS-T. Clarity™ Western ECL Blotting Substrate (BioRad) was
678 mixed at a 1:1 ratio and applied to the membrane for 5 min. Chemiluminescent signal was
679 imaged on ChemiDocTouch Chemiluminescence setting. Band intensity was quantified using
680 ImageLab software (BioRad), normalizing to total protein.

681 **Filamentous and Globular Actin Fractionation**

682 Actin stabilization and depolymerization buffer recipes were obtained from Rasmussen et
683 al. (2010) and protocol was adapted from "G- Actin / F-Actin In Vivo Assay Kit," (n.d.). Briefly,
684 following treatment, HUVECs were lysed in 100 μL actin stabilization buffer (0.1M PIPES, pH
685 = 6.9, 30% glycerol, 5% DMSO, 1mM MgSO4, 1mM EGTA, 1% Triton X-100, 1mM ATP,
686 protease inhibitor) for each well of a confluent 6-well dish. Lysates were homogenized with a
687 21-gauge needle, incubated at 30˚C for 10 min, and centrifuged at 350 xg for 5 min to remove
688 cell debris. Supernatant was then transferred to a 600 μL thick-walled centrifuge tube (Beckman,
689 California, US) and subjected to 100,000 xg ultracentrifugation for 1 h. Following
690 ultracentrifugation, the supernatant (G-actin) was mixed with 25 μL 5X SDS sample buffer (0.25
691 M Tris-Cl, pH = 6.8, 10% SDS, 50% glycerol, 0.5 M DTT and 0.25% bromophenol blue) and
692 incubated at 95˚C for 5 min. The pellet from ultracentrifugation (F-actin) was mixed with ice-
693 cold 100 μL actin depolymerization buffer (0.1 M PIPES, pH = 6.8, 1mM MgSO4, 10mM
694 CaCl2, 5 μM Cytochalasin D). The F-actin fraction was then mixed with 25 μL 5X SDS sample

695 buffer and incubated at 95°C for 5 min. Samples were subjected to protein electrophoresis and
696 immunoblotting using antibodies for β-actin.

697 **Quantitative Reverse-Transcriptase Polymerase Chain Reaction (qRT-PCR)**

698 Cells were lysed in 250 μL RLT buffer (Qiagen, Hilden, Germany) and RNA was
699 extracted using the RNeasy Plus Mini kit (Qiagen) according to the manufacturer's instructions.
700 Complementary DNA (cDNA) was synthesized from 1 μg of total RNA using the qScript cDNA
701 SuperMix (QuantaBio, Hilden, Germany) according to the manufacturer's instructions. Real-
702 time quantitative PCR with SsoFast EvaGreen qPCR MasterMix (BioRad) was used to quantify
703 the fold-change in mRNA abundance. Relative fluorescence was quantified using CFX Connect
704 (BioRad). All qRT-PCR primers efficiencies were between 90-110% in HUVECs and sequences
705 are found in Table S5.

706 **Luciferase Assay for TEAD Transcriptional Activity**

707 HEK-293A cells were seeded in antibiotic-free DMEM at 75,000 cells/well. Mixtures of
708 500 ng of the target construct (pcDNA (Vector), pcDNA-KapB (KapB), p1XFLAG or
709 p2XFLAG-YAP 5SA), 450 ng 8X-GTIIC luciferase reporter, 50 ng TREX-Renilla luciferase
710 reporter and 3 μL FuGENE HD Transfection Reagent (Promega, Madison, Wisconsin, US) were
711 transfected into HEK-293A cells. After 36 h, DMEM containing only 2 mM L-glutamine
712 (starvation media) was supplied to the cells. Twelve hours after addition of starvation media,
713 cells were lysed in 200 μL passive lysis buffer (Promega) and luciferase activity was assayed
714 using the Dual-Luciferase Reporter Assay System (Promega) according to the manufacturer's
715 instructions. Luminescence was measured using the GloMax Luminometer (Promega).

716 **Luciferase Assay for Stability of mRNA with AU-Rich Elements**

717 This technique is described in Corcoran, Khaperskyy, and McCormick (2011). Briefly,
718 Hela-Tet Off cells were seeded in antibiotic-free DMEM at 100,000 cells/well. Mixtures of 900
719 ng of the target construct (pcDNA (Vector), pcDNA-KapB (KapB), p1XFLAG or p2XFLAG-
720 YAP 5SA), 90 ng TREX-Firefly ARE luciferase, 10 ng TREX-Renilla luciferase and 3 μL
721 FuGENE HD Transfection Reagent (Promega) were transfected into Hela Tet-Off cells. After 36
722 h, 1 μg/mL doxycycline was supplied to the cells to inhibit further transcription of each reporter.
723 Twelve hours after addition of doxycycline, cells were lysed in 200 μL passive lysis buffer
724 (Promega) and luciferase activity was assayed using the Dual-Luciferase Reporter Assay System

725 (Promega) according to the manufacturer's instructions. Luminescence was measured using the
726 GloMax Luminometer (Promega).

727 **Collagen-Coating for Altering Matrix Stiffness**

728 Coverslips (no. 1.5, Electron Microscopy Sciences) were coated with a dilution series (0
729 to 64 μg/cm^2) of rat-tail collagen-1 (Gibco) in 0.02 M acetic acid for 4 h at RT. Slides were
730 sterilized with UV irradiation and washed with 2 times with sterile 1X PBS prior to seeding
731 cells.

732 **Unidirectional Fluid Flow for Endothelial Cell Shear Stress**

733 A parallel-plate flow chamber was used to expose ECs to shear stress. The system was
734 described in detail in Gomez-Garcia et al. (2018). Briefly, cleaned, unfrosted microscope slides
735 (Cole-Parmer, Vernon Hills, Illinois, US) were coated for 4 h at RT with rat-tail collagen-1
736 (Gibco) in 0.02 M acetic acid for a resultant 8.3 μg/cm^2 collagen density. Slides were sterilized
737 with UV irradiation and washed 2 times with sterile 1X PBS. HUVECs were seeded at a density
738 of 350,000 cells/slide and cultured for 24 h. Forty-five mL of EGM-2 supplemented with dextran
739 (Spectrum Chemical, New Brunswick, New Jersey, US) for a resultant 3 cP viscosity was added
740 to the stock media bottle. The stock media bottle was connected with the associated tubing and
741 pulse dampener. Slides with seeded cells were inserted onto the flow chamber, a gasket
742 (Specialty Manufacturing, Calgary, Canada) was added, and the system was sealed shut and
743 attached to the flow loop following the outlet of a pulse dampener. The rate of fluid flow was
744 started at 0.3 L/min and doubled every 15 min until final flow rates of 0.6 L/min and 2.7 L/min
745 were reached, corresponding to shear stress rates of 2 and 10 dyn/cm^2. Following 21 h, cells were
746 removed and immediately fixed for immunofluorescence or lysed for immunoblotting.

747 **Statistical Analysis**

748 Statistical analysis was performed in GraphPad Prism 8.0 software. Significance was
749 determined using a ratio paired t-test or repeated measures analysis of variance (ANOVA). One-
750 tailed ratio paired t-tests were applied in comparisons specifically examining PB restoration in
751 KapB-expressing cells as a directional hypothesis. In all other comparisons, two-tailed ratio
752 paired t-tests were applied. Significance was determined at $p = 0.05$. Each biological replicate
753 for CellProfiler quantification consisted of 6 images of each treatment in a given experiment,
754 counting approximately 100 to 200 cells per treatment.
755

References

Aizer, Adva, Yehuda Brody, Lian Wee Ler, Nahum Sonenberg, Robert H. Singer, and Yaron Shav-Tal. 2008. "The Dynamics of Mammalian P Body Transport, Assembly, and Disassembly In Vivo." *Molecular Biology of the Cell* 19 (11): 4154–66. https://doi.org/10.1091/mbc.E08.

Amano, M, K Chihara, K Kimura, Y Fukata, N Nakamura, Y Matsuura, and K Kaibuchi. 1997. "Formation of Actin Stress Fibers and Focal Adhesions Enhanced by Rho-Kinase." *Science* 275 (5304): 1308–11. https://doi.org/10.1126/science.275.5304.1308.

Amano, Mutsuki, Masaaki Ito, Kazushi Kimura, Yuko Fukata, Kazuyasu Chihara, Takeshi Nakano, Yoshiharu Matsuura, and Kozo Kaibuchi. 1996. "Phosphorylation and Activation of Myosin by Rho-Associated Kinase (Rho-Kinase)." *The Journal of Biological Chemistry* 271 (34): 20246–49. https://doi.org/10.1074/jbc.271.34.20246.

Arias, Carolina, Ben Weisburd, Noam Stern-Ginossar, Alexandre Mercier, Alexis S Madrid, Priya Bellare, Meghan Holdorf, Jonathan S. Weissman, and Don Ganem. 2014. "KSHV 2.0: A Comprehensive Annotation of the Kaposi's Sarcoma-Associated Herpesvirus Genome Using Next-Generation Sequencing Reveals Novel Genomic and Functional Features." *PLoS Pathogens* 10 (1). https://doi.org/10.1371/journal.ppat.1003847.

Asano, Yukako, and Issei Mabuchi. 2001. "Calyculin-A, an Inhibitor for Protein Phosphatases, Induces Cortical Contraction in Unfertilized Sea Urchin Eggs." *Cell Motility and the Cytoskeleton* 48 (4): 245–61. https://doi.org/10.1002/cm.1013.

Bakheet, Tala, Edward Hitti, and Khalid S A Khabar. 2017. "ARED-Plus: An Updated and Expanded Database of AU-Rich Element-Containing MRNAs and Pre-MRNAs." *Nucleic Acids Research* 46 (October 2017): 2017–19. https://doi.org/10.1093/nar/gkx975.

Bakheet, Tala, Bryan R G Williams, and Khalid S A Khabar. 2006. "ARED 3.0: The Large and Diverse AU-Rich Transcriptome." *Nucleic Acids Research* 34 (Database issue): D111–14. https://doi.org/10.1093/nar/gkj052.

Balinsky, Corey A, Hana Schmeisser, Alexandra I Wells, Sundar Ganesan, Tengchuan Jin, Kavita Singh, and Kathryn C Zoon. 2017. "IRAV (FLJ11286), an Interferon-Stimulated Gene with Antiviral Activity against Dengue Virus, Interacts with MOV10." Edited by Michael S. Diamond. *Journal of Virology* 91 (5). https://doi.org/10.1128/JVI.01606-16.

Blanco, Fernando F, Sandhya Sanduja, Natasha G Deane, Perry J Blackshear, and Dan A Dixon.

787 2014. “Transforming Growth Factor β Regulates P-Body Formation through Induction of
788 the MRNA Decay Factor Tristetraprolin.” *Molecular and Cellular Biology* 34 (2): 180–95.
789 https://doi.org/10.1128/MCB.01020-13.
790 Boshoff, Chris, Thomas F Schulz, Margaret M Kennedy, Andrew K Graham, Cyril Fisher, Alero
791 Thomas, J O’D. McGee, Robin a Weiss, and John J O’Leary. 1995. “Kaposi’s Sarcoma-
792 Associated Herpesvirus Infects Endothelial and Spindle Cells.” *Nature Medicine* 1 (12):
793 1274–78. https://doi.org/10.1038/nm1295-1274.
794 Bubb, Michael R, Ilan Spector, Bret B Beyer, and Katina M Fosen. 2000. “Effects of
795 Jasplakinolide on the Kinetics of Actin Polymerization.” *Journal of Biological Chemistry*
796 275 (7): 5163–70. https://doi.org/10.1074/jbc.275.7.5163.
797 Bunnell, Tina M, Brandon J Burbach, Yoji Shimizu, and James M Ervasti. 2011. “β-Actin
798 Specifically Controls Cell Growth, Migration, and the G-Actin Pool.” Edited by Paul
799 Forscher. *Molecular Biology of the Cell* 22 (21): 4047–58. https://doi.org/10.1091/mbc.e11-
800 06-0582.
801 Burdick, Ryan, Jessica L Smith, Chawaree Chaipan, Yeshitila Friew, Jianbo Chen, Narasimhan J
802 Venkatachari, Krista A Delviks-Frankenberry, Wei-Shau Hu, and Vinay K. Pathak. 2010.
803 “P Body-Associated Protein Mov10 Inhibits HIV-1 Replication at Multiple Stages.”
804 *Journal of Virology* 84 (19): 10241–53. https://doi.org/10.1128/jvi.00585-10.
805 Burgess, Hannah M., and Ian Mohr. 2015. “Cellular 5′-3′ MRNA Exonuclease Xrn1 Controls
806 Double-Stranded RNA Accumulation and Anti-Viral Responses.” *Cell Host and Microbe*
807 17 (3): 332–44. https://doi.org/10.1016/j.chom.2015.02.003.
808 Burridge, Keith, and Christophe Guilluy. 2016. “Focal Adhesions, Stress Fibers and Mechanical
809 Tension.” *Experimental Cell Research* 343 (1): 14–20.
810 https://doi.org/10.1016/j.yexcr.2015.10.029.
811 Carroll, Bernadette, Noor Mohd-Naim, Filipe Maximiano, Marieke A. Frasa, Jessica
812 McCormack, Mattea Finelli, Sigrid B. Thoresen, et al. 2013. “The TBC/RabGAP Armus
813 Coordinates Rac1 and Rab7 Functions during Autophagy.” *Developmental Cell* 25 (1): 15–
814 28. https://doi.org/10.1016/j.devcel.2013.03.005.
815 Calvo, Fernando, Nil Ege, Araceli Grande-Garcia, Steven Hooper, Robert P. Jenkins, Shahid I.
816 Chaudhry, Kevin Harrington, et al. 2013. “Mechanotransduction and YAP-Dependent
817 Matrix Remodelling Is Required for the Generation and Maintenance of Cancer-Associated

818 Fibroblasts." *Nature Cell Biology* 15 (6): 637–46. https://doi.org/10.1038/ncb2756.
819 Chai, J, and Andrzej S Tarnawski. 2002. "Serum Response Factor: Discovery, Biochemistry,
820 Biological Roles and Implications for Tissue Injury Healing." *Journal of Physiology and*
821 *Pharmacology* 53 (2): 147–57. https://doi.org/10.1007/s12630-011-9636-x.
822 Chambers, Joseph E, Lucy E Dalton, Hanna J Clarke, Elke Malzer, Caia S Dominicus, Vruti
823 Patel, Greg Moorhead, David Ron, and Stefan J Marciniak. 2015. "Actin Dynamics Tune
824 the Integrated Stress Response by Regulating Eukaryotic Initiation Factor 2α
825 Dephosphorylation." *ELife* 4 (March). https://doi.org/10.7554/eLife.04872.
826 Chang, Y, E Cesarman, M S Pessin, F Lee, J Culpepper, D M Knowles, and P S Moore. 1994.
827 "Identification of Herpes-like DNA Sequences in AIDS-Associated Kaposi's Sarcoma."
828 *Science* 266: 1865–69. https://doi.org/10.1126/science.7997879.
829 Chen, C Y, and A B Shyu. 1995. "AU-Rich Elements: Characterization and Importance in
830 MRNA Degradation." *Trends in Biochemical Sciences* 20 (11): 465–70.
831 https://doi.org/10.1016/S0968-0004(00)89102-1.
832 Ciufo, D M, J S Cannon, L J Poole, F Y Wu, P Murray, R F Ambinder, and G S Hayward. 2001.
833 "Spindle Cell Conversion by Kaposi's Sarcoma-Associated Herpesvirus: Formation of
834 Colonies and Plaques with Mixed Lytic and Latent Gene Expression in Infected Primary
835 Dermal Microvascular EndCiufo, D. M., Cannon, J. S., Poole, L. J., Wu, F. Y., Murray,
836 P.,." *Journal of Virology* 75 (12): 5614–26. https://doi.org/10.1128/JVI.75.12.5614-
837 5626.2001.
838 Corcoran, Jennifer A, Benjamin P Johnston, and Craig McCormick. 2015. "Viral Activation of
839 MK2-Hsp27-P115RhoGEF-RhoA Signaling Axis Causes Cytoskeletal Rearrangements, P-
840 Body Disruption and ARE-MRNA Stabilization." Edited by Erle S. Robertson. *PLoS*
841 *Pathogens* 11 (1): e1004597. https://doi.org/10.1371/journal.ppat.1004597.
842 Corcoran, Jennifer A, Denys A Khaperskyy, Benjamin P Johnston, Christine A King, David P.
843 Cyr, Alisha V. Olsthoorn, and Craig McCormick. 2012. "Kaposi's Sarcoma-Associated
844 Herpesvirus G-Protein-Coupled Receptor Prevents AU-Rich-Element-Mediated MRNA
845 Decay." *Journal of Virology* 86 (16): 8859–71. https://doi.org/10.1128/JVI.00597-12.
846 Corcoran, Jennifer A, Denys A. Khaperskyy, and Craig McCormick. 2011. "Assays for
847 Monitoring Viral Manipulation of Host ARE-MRNA Turnover." *Methods* 55 (2): 172–81.
848 https://doi.org/10.1016/j.ymeth.2011.08.005.

849 Corcoran, Jennifer A, and Craig McCormick. 2015. "Viral Activation of Stress-Regulated Rho-
850 GTPase Signaling Pathway Disrupts Sites of MRNA Degradation to Influence Cellular
851 Gene Expression." *Small GTPases* 6 (4): 178–85.
852 https://doi.org/10.1080/21541248.2015.1093068.
853 Cramer, Louise P, Margaret Siebert, and Timothy J Mitchison. 1997. "Identification of Novel
854 Graded Polarity Actin Filament Bundles in Locomoting Heart Fibroblasts: Implications for
855 the Generation of Motile Force." *Journal of Cell Biology* 136 (6): 1287–1305.
856 https://doi.org/10.1083/jcb.136.6.1287.
857 Cuevas, Rolando A, Arundhati Ghosh, Christina Wallerath, Veit Hornung, Carolyn B Coyne,
858 and Saumendra N Sarkar. 2016. "MOV10 Provides Antiviral Activity against RNA Viruses
859 by Enhancing RIG-I–MAVS-Independent IFN Induction." *The Journal of Immunology* 196
860 (9): 3877–86. https://doi.org/10.4049/jimmunol.1501359.
861 Das, Joyjyoti, Somnath Maji, Tarun Agarwal, Suman Chakraborty, and Tapas K Maiti. 2018.
862 "Hemodynamic Shear Stress Induces Protective Autophagy in HeLa Cells through Lipid
863 Raft-Mediated Mechanotransduction." *Clinical and Experimental Metastasis* 35 (3): 135–
864 48. https://doi.org/10.1007/s10585-018-9887-9.
865 Docena, G, L Rovedatti, L Kruidenier, Á Fanning, NAB Leakey, CH Knowles, K Lee, et al.
866 2010. "Down-Regulation of P38 Mitogen-Activated Protein Kinase Activation and
867 Proinflammatory Cytokine Production by Mitogen-Activated Protein Kinase Inhibitors in
868 Inflammatory Bowel Disease." *Clinical and Experimental Immunology* 162 (1): 108–15.
869 https://doi.org/10.1111/j.1365-2249.2010.04203.x.
870 Dupont, Sirio, Leonardo Morsut, Mariaceleste Aragona, Elena Enzo, Stefano Giulitti,
871 Michelangelo Cordenonsi, Francesca Zanconato, et al. 2011. "Role of YAP/TAZ in
872 Mechanotransduction." *Nature* 474 (7350): 179–83. https://doi.org/10.1038/nature10137.
873 Edlund, Magnus, Marc A Lotano, and Carol A Otey. 2001. "Dynamics of Alpha-Actinin in Focal
874 Adhesions and Stress Fibers Visualized with Alpha-Actinin-Green Fluorescent Protein."
875 *Cell Motility and the Cytoskeleton* 48 (3): 190–200. https://doi.org/10.1002/1097-
876 0169(200103)48:3<190::AID-CM1008>3.0.CO;2-C.
877 Ensoli, B. 1998. "Kaposi's Sarcoma: A Result of the Interplay among Inflammatory Cytokines,
878 Angiogenic Factors and Viral Agents." *Cytokine & Growth Factor Reviews* 9 (1): 63–83.
879 https://doi.org/10.1016/S1359-6101(97)00037-3.

880 Eulalio, Ana, Isabelle Behm-Ansmant, and Elisa Izaurralde. 2007. "P Bodies: At the Crossroads
881 of Post-Transcriptional Pathways." *Nature Reviews Molecular Cell Biology* 8 (1): 9–22.
882 https://doi.org/10.1038/nrm2080.
883 Finch-Edmondson, Megan, and Marius Sudol. 2016. "Framework to Function: Mechanosensitive
884 Regulators of Gene Transcription." *Cellular & Molecular Biology Letters* 21 (1): 28.
885 https://doi.org/10.1186/s11658-016-0028-7.
886 Franks, Tobias M, and Jens Lykke-Andersen. 2007. "TTP and BRF Proteins Nucleate Processing
887 Body Formation to Silence MRNAs with AU-Rich Elements." *Genes and Development* 21
888 (6): 719–35. https://doi.org/10.1101/gad.1494707.
889 Friedland, Julie C, Mark H Lee, and David Boettiger. 2009. "Mechanically Activated Integrin
890 Switch Controls Alpha5 Beta1 Function." *Science* 323 (January): 642–44.
891 "G-Actin / F-Actin In Vivo Assay Kit." n.d. Cytoskeleton Inc.
892 Ganem, Don. 1997. "KSHV and Kaposi's Sarcoma: The End of the Beginning?" *Cell* 91 (2):
893 157–60. https://doi.org/10.1016/S0092-8674(00)80398-0.
894 Garcia, Melissa C, Denise M Ray, Brad Lackford, Mark Rubino, Kenneth Olden, and John D
895 Roberts. 2009. "Arachidonic Acid Stimulates Cell Adhesion through a Novel P38 MAPK-
896 RhoA Signaling Pathway That Involves Heat Shock Protein 27." *Journal of Biological*
897 *Chemistry* 284 (31): 20936–45. https://doi.org/10.1074/jbc.M109.020271.
898 Gomez-Garcia, M Juliana, Amber L Doiron, Robyn RM Steele, Hagar I Labouta, Bahareh
899 Vafadar, Robert D Shepherd, Ian D Gates, David T Cramb, Sarah J Childs, and Kristina D
900 Rinker. 2018. "Nanoparticle Localization in Blood Vessels: Dependence on Fluid Shear
901 Stress, Flow Disturbances, and Flow-Induced Changes in Endothelial Physiology."
902 *Nanoscale* 10 (32): 15249–61. https://doi.org/10.1039/C8NR03440K.
903 Grashoff, Carsten, Brenton D Hoffman, Michael D Brenner, Ruobo Zhou, Maddy Parsons,
904 Michael T Yang, Mark A McLean, et al. 2010. "Measuring Mechanical Tension across
905 Vinculin Reveals Regulation of Focal Adhesion Dynamics." *Nature* 466 (7303): 263–66.
906 https://doi.org/10.1038/nature09198.
907 Grossmann, Claudia, Simona Podgrabinska, Mihaela Skobe, and Don Ganem. 2006. "Activation
908 of NF-KB by the Latent VFLIP Gene of Kaposi's Sarcoma-Associated Herpesvirus Is
909 Required for the Spindle Shape of Virus-Infected Endothelial Cells and Contributes to Their
910 Proinflammatory Phenotype." *Journal of Virology* 80 (14): 7179–85.

911 https://doi.org/10.1128/jvi.01603-05.
912 Halder, Georg, Sirio Dupont, and Stefano Piccolo. 2012. "Transduction of Mechanical and
913 Cytoskeletal Cues by YAP and TAZ." *Nature Publishing Group* 13 (9): 591–600.
914 https://doi.org/10.1038/nrm3416.
915 Hardy, Shana D, Aparna Shinde, Wen Horng Wang, Michael K Wendt, and Robert L Geahlen.
916 2017. "Regulation of Epithelial-Mesenchymal Transition and Metastasis by TGF-β, P-
917 Bodies, and Autophagy." *Oncotarget* 8 (61): 103302–14.
918 https://doi.org/10.18632/oncotarget.21871.
919 Honda, K, T Yamada, R Endo, Y Ino, M Gotoh, H Tsuda, Y Yamada, H Chiba, and S Hirohashi.
920 1998. "Actinin-4, a Novel Actin-Bundling Protein Associated with Cell Motility and Cancer
921 Invasion.[Erratum Appears in J Cell Biol 1998 Oct 5;143(1):Following 276]." *Journal of*
922 *Cell Biology* 140 (6): 1383–93. https://doi.org/10.1083/jcb.140.6.1383.
923 Honda, Kazufumi. 2015. "The Biological Role of Actinin-4 (ACTN4) in Malignant Phenotypes
924 of Cancer." *Cell and Bioscience* 5 (1): 1–9. https://doi.org/10.1186/s13578-015-0031-0.
925 Horvathova I, Voigt F, Kotrys A V., Zhan Y, Artus-Revel CG, Eglinger J, et al. 2017. "The
926 Dynamics of mRNA Turnover Revealed by Single-Molecule Imaging in Single Cells."
927 *Molecular Cell* 68 (3):615-625. https://doi.org/10.1016/j.molcel.2017.09.030
928 Hotulainen, Pirta, and Pekka Lappalainen. 2006. "Stress Fibers Are Generated by Two Distinct
929 Actin Assembly Mechanisms in Motile Cells." *Journal of Cell Biology* 173 (3): 383–94.
930 https://doi.org/10.1083/jcb.200511093.
931 Huang, Yu, Li Wang, Jiang Yun Luo, Bochuan Li, Xiao Yu Tian, Li Jing Chen, Yuhong Huang,
932 et al. 2016. "Integrin-YAP/TAZ-JNK Cascade Mediates Atheroprotective Effect of
933 Unidirectional Shear Flow." *Nature* 540 (7634): 579–82.
934 https://doi.org/10.1038/nature20602.
935 Hubstenberger, Arnaud, Maïté Courel, Marianne Bénard, Sylvie Souquere, Michèle Ernoult-
936 Lange, Racha Chouaib, Zhou Yi, et al. 2017. "P-Body Purification Reveals the
937 Condensation of Repressed MRNA Regulons." *Molecular Cell* 68 (1): 144-157.e5.
938 https://doi.org/10.1016/j.molcel.2017.09.003.
939 Ishizaki, T, M Uehata, I Tamechika, J Keel, K Nonomura, M Maekawa, and S Narumiya. 2000.
940 "Pharmacological Properties of Y-27632, a Specific Inhibitor of Rho-Associated Kinases."
941 *Molecular Pharmacology* 57 (5): 976–83. http://www.ncbi.nlm.nih.gov/pubmed/10779382.

942 Jackson, Wesley M, Michael J Jaasma, Andrew D Baik, and Tony M Keaveny. 2008. "Over-
943 Expression of Alpha-Actinin with a GFP Fusion Protein Is Sufficient to Increase Whole-
944 Cell Stiffness in Human Osteoblasts." *Annals of Biomedical Engineering* 36 (10): 1605–14.
945 https://doi.org/10.1007/s10439-008-9533-9.
946 Jang, Wonyul, Tackhoon Kim, Ja Seung Koo, Sang-kyum Kim, and Dae-Sik Lim. 2017. "
947 Mechanical Cue-induced YAP Instructs Skp2-dependent Cell Cycle Exit and Oncogenic
948 Signaling ." *The EMBO Journal* 36 (17): 2510–28.
949 https://doi.org/10.15252/embj.201696089.
950 Joshi, Jyotsna, Gautam Mahajan, and Chandrasekhar R. Kothapalli. 2018. "Three-Dimensional
951 Collagenous Niche and Azacytidine Selectively Promote Time-Dependent
952 Cardiomyogenesis from Human Bone Marrow-Derived MSC Spheroids." *Biotechnology*
953 *and Bioengineering* 115 (8): 2013–26. https://doi.org/10.1002/bit.26714.
954 Julian, Linda, and Michael F Olson. 2014. "Rho-Associated Coiled-Coil Containing Kinases
955 (ROCK)." *Small GTPases* 5 (2): e29846. https://doi.org/10.4161/sgtp.29846.
956 Kamentsky, Lee, Thouis R Jones, Adam Fraser, Mark-Anthony Bray, David J Logan, Katherine
957 L Madden, Vebjorn Ljosa, Curtis Rueden, Kevin W Eliceiri, and Anne E Carpenter. 2011.
958 "Improved Structure, Function and Compatibility for CellProfiler: Modular High-
959 Throughput Image Analysis Software." *Bioinformatics (Oxford, England)* 27 (8): 1179–80.
960 https://doi.org/10.1093/bioinformatics/btr095.
961 Kapoor, Avnish, Wantong Yao, Haoqiang Ying, Sujun Hua, Alison Liewen, Qiuyun Wang, Yi
962 Zhong, et al. 2014. "Yap1 Activation Enables Bypass of Oncogenic KRAS Addiction in
963 Pancreatic Cancer." *Cell* 158 (1): 185–97. https://doi.org/10.1016/j.cell.2014.06.003.
964 Katoh, K, Y Kano, M Masuda, H Onishi, and K Fujiwara. 1998. "Isolation and Contraction of
965 the Stress Fiber." *Molecular Biology of the Cell* 9 (7): 1919–38.
966 https://doi.org/10.1091/mbc.9.7.1919.
967 Kedersha, Nancy, and Paul Anderson. 2007. "Mammalian Stress Granules and Processing
968 Bodies." *Methods in Enzymology* 431 (07): 61–81. https://doi.org/10.1016/S0076-
969 6879(07)31005-7.
970 Kedersha, Nancy, Sarah Tisdale, Tyler Hickman, and Paul Anderson. 2008. *Chapter 26 Real-*
971 *Time and Quantitative Imaging of Mammalian Stress Granules and Processing Bodies*.
972 *Methods in Enzymology*. 1st ed. Vol. 448. Elsevier Inc. https://doi.org/10.1016/S0076-

973 6879(08)02626-8.
974 Kimura, K, M Ito, M Amano, K Chihara, Y Fukata, M Nakafuku, B Yamamori, et al. 1996.
975 "Regulation of Myosin Phosphatase by Rho and Rho-Associated Kinase (Rho-Kinase)."
976 *Science (New York, N.Y.)* 273 (5272): 245–48.
977 https://doi.org/10.1126/science.273.5272.245.
978 Kimura, Masahiro, Takahiro Horie, Osamu Baba, Yuya Ide, Shuhei Tsuji, Randolph Ruiz
979 Rodriguez, Toshimitsu Watanabe, et al. 2020. "Homeobox A4 Suppresses Vascular
980 Remodeling by Repressing YAP/TEAD Transcriptional Activity." *EMBO Reports* 21 (4):
981 e48389. https://doi.org/10.15252/embr.201948389.
982 Kong, Fang, Andrés J García, A Paul Mould, Martin J Humphries, and Cheng Zhu. 2009.
983 "Demonstration of Catch Bonds between an Integrin and Its Ligand." *Journal of Cell*
984 *Biology* 185 (7): 1275–84. https://doi.org/10.1083/jcb.200810002.
985 Kovac, Bianca. 2010. "Role and Function of Nonmuscle Alpha-Actinin-1 and -4 in Regulating
986 Distinct Subcategories of Actin Stress Fibers in Mammalian Cells." University of Helsinki.
987 Kovacs, M, J Toth, C Hetenyi, A Malnasi-Csizmadia, and JR Sellers. 2004. "Mechanism of
988 Blebbistatin Inhibition of Myosin II." *Journal of Biological Chemistry* 279 (34): 35557–63.
989 https://doi.org/10.1074/jbc.M405319200.
990 Lai, Jason Kuan Han, and Didier Y.R. Stainier. 2017. "Pushing Yap into the Nucleus with Shear
991 Force." *Developmental Cell* 40 (6): 517–18. https://doi.org/10.1016/j.devcel.2017.03.008.
992 Lazarides, Elias, and Keith Burridge. 1975. "α-Actinin: Immunofluorescent Localization of a
993 Muscle Structural Protein in Nonmuscle Cells." *Cell* 6 (3): 289–98.
994 https://doi.org/10.1016/0092-8674(75)90180-4.
995 Lee, Byoungkoo, Xin Zhou, Kristin Riching, Kevin W Eliceiri, Patricia J Keely, Scott A
996 Guelcher, Alissa M Weaver, and Yi Jiang. 2014. "A Three-Dimensional Computational
997 Model of Collagen Network Mechanics." Edited by Sanjay Kumar. *PLoS ONE* 9 (11):
998 e111896. https://doi.org/10.1371/journal.pone.0111896.
999 Lee, Hyun Jung, Miguel F Diaz, Katherine M Price, Joyce A Ozuna, Songlin Zhang, Eva M
1000 Sevick-Muraca, John P. Hagan, and Pamela L. Wenzel. 2017. "Fluid Shear Stress Activates
1001 YAP1 to Promote Cancer Cell Motility." *Nature Communications* 8 (1): 14122.
1002 https://doi.org/10.1038/ncomms14122.
1003 Lee, JSH. 2006. "Ballistic Intracellular Nanorheology Reveals ROCK-Hard Cytoplasmic

1004 Stiffening Response to Fluid Flow." *Journal of Cell Science* 119 (9): 1760–68.
1005 https://doi.org/10.1242/jcs.02899.
1006 Lee, Stacey, and Sanjay Kumar. 2016. "Actomyosin Stress Fiber Mechanosensing in 2D and
1007 3D." *F1000Research* 5 (0): 2261. https://doi.org/10.12688/f1000research.8800.1.
1008 Li, Ying, Rui Chen, Qian Zhou, Zhisheng Xu, Chao Li, Shuai Wang, Aiping Mao, Xiaodong
1009 Zhang, Weiwu He, and Hong Bing Shu. 2012. "LSm14A Is a Processing Body-Associated
1010 Sensor of Viral Nucleic Acids That Initiates Cellular Antiviral Response in the Early Phase
1011 of Viral Infection." *Proceedings of the National Academy of Sciences of the United States of*
1012 *America* 109 (29): 11770–75. https://doi.org/10.1073/pnas.1203405109.
1013 Liu, G, FX Yu, YC Kim, Z. Meng, J Naipauer, DJ Looney, X Liu, JS Gutkind, EA Mesri, and K
1014 L Guan. 2015. "Kaposi Sarcoma-Associated Herpesvirus Promotes Tumorigenesis by
1015 Modulating the Hippo Pathway." *Oncogene* 34 (27): 3536–46.
1016 https://doi.org/10.1038/onc.2014.281.
1017 Liu, Huan, Xiaoming Dai, Xiaolei Cao, Huan Yan, Xinyan Ji, Haitao Zhang, Shuying Shen, et al.
1018 2018. "PRDM4 Mediates YAP-induced Cell Invasion by Activating Leukocyte-specific
1019 Integrin B2 Expression." *EMBO Reports* 19 (6): 1–14.
1020 https://doi.org/10.15252/embr.201745180.
1021 Liu, J, X Bi, T Chen, Q Zhang, SX Wang, JJ Chiu, GS Liu, Y Zhang, P Bu, and F. Jiang. 2015.
1022 "Shear Stress Regulates Endothelial Cell Autophagy via Redox Regulation and Sirt1
1023 Expression." *Cell Death and Disease* 6 (7). https://doi.org/10.1038/cddis.2015.193.
1024 Liu, Zeming, Wen Zeng, Shi Wang, Xiangwang Zhao, Yawen Guo, Pan Yu, Xingjie Yin,
1025 Chunping Liu, and Tao Huang. 2017. "A Potential Role for the Hippo Pathway Protein,
1026 YAP, in Controlling Proliferation, Cell Cycle Progression, and Autophagy in BCPAP and
1027 KI Thyroid Papillary Carcinoma Cells." *American Journal of Translational Research* 9 (7):
1028 3212–23.
1029 Lumb, Jennifer H, Lauren M Popov, Siyuan Ding, Marie T Keith, Bryan D Merrill, Harry B
1030 Greenberg, Jan E. Carette, Qin Li, and Jin Billy Li. 2017. "DDX6 Represses Aberrant
1031 Activation of Interferon-Stimulated Genes." *Cell Reports* 20 (4): 819–31.
1032 https://doi.org/10.1016/j.celrep.2017.06.085.
1033 Mauvezin, Caroline, and Thomas P Neufeld. 2015. "Bafilomycin A1 Disrupts Autophagic Flux
1034 by Inhibiting Both." *Autophagy* 11 (8): 1437–38.

1035 McCormick, Craig, and Don Ganem. 2005. "The Kaposin B Protein of KSHV Activates the
1036 P38/MK2 Pathway and Stabilizes Cytokine MRNAs." *Science* 307 (5710): 739–41.
1037 https://doi.org/10.1126/science.1105779.
1038 Mo, Jung Soon, Zhipeng Meng, Young Chul Kim, Hyun Woo Park, Carsten Gram Hansen,
1039 Soohyun Kim, Dae Sik Lim, and Kun Liang Guan. 2015. "Cellular Energy Stress Induces
1040 AMPK-Mediated Regulation of YAP and the Hippo Pathway." *Nature Cell Biology* 17 (4):
1041 500–510. https://doi.org/10.1038/ncb3111.
1042 Montaner, Silvia, Akrit Sodhi, Amanda K. Ramsdell, Daniel Martin, Jiadi Hu, Earl T Sawai, and
1043 J. Silvio Gutkind. 2006. "The Kaposi's Sarcoma-Associated Herpesvirus G Protein-Coupled
1044 Receptor as a Therapeutic Target for the Treatment of Kaposi's Sarcoma." *Cancer*
1045 *Research* 66 (1): 168–74. https://doi.org/10.1158/0008-5472.CAN-05-1026.
1046 Moreno-Vicente, Roberto, Dácil María Pavón, Inés Martín-Padura, Mauro Català-Montoro,
1047 Alberto Díez-Sánchez, Antonio Quílez-Álvarez, Juan Antonio López, et al. 2018.
1048 "Caveolin-1 Modulates Mechanotransduction Responses to Substrate Stiffness through
1049 Actin-Dependent Control of YAP." *Cell Reports* 25 (6): 1622-1635.e6.
1050 https://doi.org/10.1016/j.celrep.2018.10.024.
1051 Nakajima, Hiroyuki, and Naoki Mochizuki. 2017. "Flow Pattern-Dependent Endothelial Cell
1052 Responses through Transcriptional Regulation." *Cell Cycle* 16 (20): 1893–1901.
1053 https://doi.org/10.1080/15384101.2017.1364324.
1054 Nakajima, Hiroyuki, Kimiko Yamamoto, Sobhika Agarwala, Kenta Terai, Hajime Fukui,
1055 Shigetomo Fukuhara, Koji Ando, et al. 2017. "Flow-Dependent Endothelial YAP
1056 Regulation Contributes to Vessel Maintenance." *Developmental Cell* 40 (6): 523-536.e6.
1057 https://doi.org/10.1016/j.devcel.2017.02.019.
1058 Naranatt, Pramod P, Shaw M. Akula, Christopher A Zien, Harinivas H Krishnan, and Bala
1059 Chandran. 2003. "Kaposi's Sarcoma-Associated Herpesvirus Induces the
1060 Phosphatidylinositol 3-Kinase-PKC-ζ-MEK-ERK Signaling Pathway in Target Cells Early
1061 during Infection: Implications for Infectivity." *Journal of Virology* 77 (2): 1524–39.
1062 https://doi.org/10.1128/jvi.77.2.1524-1539.2003.
1063 Ng, Chen Seng, Dacquin M Kasumba, Takashi Fujita, and Honglin Luo. 2020. "Spatio-Temporal
1064 Characterization of the Antiviral Activity of the XRN1-DCP1/2 Aggregation against
1065 Cytoplasmic RNA Viruses to Prevent Cell Death." *Cell Death and Differentiation*.

1066 https://doi.org/10.1038/s41418-020-0509-0.
1067 Noria, Sabrena, Feng Xu, Shannon McCue, Mara Jones, Avrum I Gotlieb, and B Lowell
1068 Langille. 2004. "Assembly and Reorientation of Stress Fibers Drives Morphological
1069 Changes to Endothelial Cells Exposed to Shear Stress." *The American Journal of Pathology*
1070 164 (4): 1211–23. https://doi.org/10.1016/S0002-9440(10)63209-9.
1071 Núñez, Rocío Daviña, Matthias Budt, Sandra Saenger, Katharina Paki, Ulrike Arnold, Anne
1072 Sadewasser, and Thorsten Wolff. 2018. "The RNA Helicase DDX6 Associates with RIG-I
1073 to Augment Induction of Antiviral Signaling." *International Journal of Molecular Sciences*
1074 19 (7): 1–14. https://doi.org/10.3390/ijms19071877.
1075 Ohashi, Kazumasa, Kyoko Nagata, Midori Maekawa, Toshimasa Ishizaki, Shuh Narumiya, and
1076 Kensaku Mizuno. 2000. "Rho-Associated Kinase ROCK Activates LIM-Kinase 1 by
1077 Phosphorylation at Threonine 508 within the Activation Loop." *Journal of Biological*
1078 *Chemistry* 275 (5): 3577–82. https://doi.org/10.1074/jbc.275.5.3577.
1079 Ojala, Päivi M, and Thomas F Schulz. 2014. "Manipulation of Endothelial Cells by KSHV:
1080 Implications for Angiogenesis and Aberrant Vascular Differentiation." *Seminars in Cancer*
1081 *Biology* 26 (June): 69–77. https://doi.org/10.1016/j.semcancer.2014.01.008.
1082 Ostareck, Dirk H, Isabel S Naarmann-de Vries, and Antje Ostareck-Lederer. 2014. "DDX6 and
1083 Its Orthologs as Modulators of Cellular and Viral RNA Expression." *Wiley Interdisciplinary*
1084 *Reviews: RNA* 5 (5): 659–78. https://doi.org/10.1002/wrna.1237.
1085 Panciera, Tito, Luca Azzolin, Atsushi Fujimura, Daniele Di Biagio, Chiara Frasson, Silvia
1086 Bresolin, Sandra Soligo, et al. 2016. "Induction of Expandable Tissue-Specific
1087 Stem/Progenitor Cells through Transient Expression of YAP/TAZ." *Cell Stem Cell* 19 (6):
1088 725–37. https://doi.org/10.1016/j.stem.2016.08.009.
1089 Pavel, Mariana, Maurizio Renna, So Jung Park, Fiona M Menzies, Thomas Ricketts, Jens
1090 Füllgrabe, Avraham Ashkenazi, et al. 2018. "Contact Inhibition Controls Cell Survival and
1091 Proliferation via YAP/TAZ-Autophagy Axis." *Nature Communications* 9 (1).
1092 https://doi.org/10.1038/s41467-018-05388-x.
1093 Pei, Tianjiao, Xin Huang, Ying Long, Changling Duan, Tingting Liu, Yujing Li, and Wei Huang.
1094 2019. "Increased Expression of YAP Is Associated with Decreased Cell Autophagy in the
1095 Eutopic Endometrial Stromal Cells of Endometriosis." *Molecular and Cellular*
1096 *Endocrinology* 491 (April): 110432. https://doi.org/10.1016/j.mce.2019.04.012.

1097 Pellegrin, S, and H Mellor. 2007. "Actin Stress Fibres." *Journal of Cell Science* 120 (20): 3491–
1098 99. https://doi.org/10.1242/jcs.018473.
1099 Pollard, Thomas D. 2016. "Actin and Actin-Binding Proteins." *Cold Spring Harbor Perspectives*
1100 *in Biology* 8 (8): a018226. https://doi.org/10.1101/cshperspect.a018226.
1101 Rasmussen, Izabela, Line H Pedersen, Luise Byg, Kazuhiro Suzuki, Hideki Sumimoto, and
1102 Frederik Vilhardt. 2010. "Effects of F/G-Actin Ratio and Actin Turn-over Rate on NADPH
1103 Oxidase Activity in Microglia." *BMC Immunology* 11 (1): 44. https://doi.org/10.1186/1471-
1104 2172-11-44.
1105 Ridley, Anne J, and Alan Hall. 1992. "The Small GTP-Binding Protein Rho Regulates the
1106 Assembly of Focal Adhesions and Actin Stress Fibers in Response to Growth Factors." *Cell*
1107 70 (3): 389–99. https://doi.org/10.1016/0092-8674(92)90163-7.
1108 Rio, Armando del, Raul Perez-Jimenez, Ruchuan Liu, Pere Roca-Cusachs, Julio M Fernandez,
1109 and Michael P Sheetz. 2009. "Stretching Single Talin Rod." *Science* 323 (5914): 638–41.
1110 Robinson, Carolyn-Ann, Gillian K Singh, Elizabeth L Castle, Bre Q Boudreau, and Jennifer A
1111 Corcoran. 2021. "A Viral Protein Utilizes the NDP52/CALCOCO2 Selective Autophagy
1112 Receptor to Disassemble Processing Bodies." *BioRxiv*, January.
1113 https://doi.org/10.1101/2021.02.07.430164.
1114 Rotsch, Christian, and Manfred Radmacher. 2000. "Drug-Induced Changes of Cytoskeletal
1115 Structure and Mechanics in Fibroblasts: An Atomic Force Microscopy Study." *Biophysical*
1116 *Journal* 78 (1): 520–35. https://doi.org/10.1016/S0006-3495(00)76614-8.
1117 Russo, James J, Roy A Bohenzky, MC Chien, Jing Chen, Ming Yan, Dawn Maddalena, J Preston
1118 Parry, et al. 1996. "Nucleotide Sequence of the Kaposi Sarcoma-Associated Herpesvirus
1119 (HHV8)." *Proceedings of the National Academy of Sciences* 93 (25): 14862–67.
1120 https://doi.org/10.1073/pnas.93.25.14862.
1121 Schmitz, Arndt AP, Eve-Ellen Govek, Benjamin Böttner, and Linda Van Aelst. 2000. "Rho
1122 GTPases: Signaling, Migration, and Invasion." *Experimental Cell Research* 261 (1): 1–12.
1123 https://doi.org/10.1006/excr.2000.5049.
1124 Sharma, Nishi R, Vladimir Majerciak, Michael J Kruhlak, Lulu Yu, Jeong Gu Kang, Acong
1125 Yang, Shuo Gu, Marvin J Fritzler, and Zhi-ming Zheng. 2019. "KSHV RNA-Binding
1126 Protein ORF57 Inhibits P-Body Formation to Promote Viral Multiplication by Interaction

with Ago2 and GW182," 1–18. https://doi.org/10.1093/nar/gkz683.

Shaw, Gray, and Robert Kamen. 1986. "A Conserved AU Sequence from the 3′ Untranslated Region of GM-CSF MRNA Mediates Selective MRNA Degradation." *Cell* 46 (5): 659–67. https://doi.org/10.1016/0092-8674(86)90341-7.

Shen, Zhewei, and Ben Z Stanger. 2015. "YAP Regulates S-Phase Entry in Endothelial Cells." Edited by Deanna M Koepp. *PLOS ONE* 10 (1): e0117522. https://doi.org/10.1371/journal.pone.0117522.

Sheth, Ujwal. 2003. "Decapping and Decay of Messenger RNA Occur in Cytoplasmic Processing Bodies." *Science* 300 (5620): 805–8. https://doi.org/10.1126/science.1082320.

Shyu, AB, ME Greenberg, and JG Belasco. 1989. "The C-Fos Transcript Is Targeted for Rapid Decay by Two Distinct MRNA Degradation Pathways." *Genes & Development* 3 (1): 60–72. https://doi.org/10.1101/gad.3.1.60.

Small, J Victor, K Rottner, I Kaverina, and KI Anderson. 1998. "Assembling an Actin Cytoskeleton for Cell Attachment and Movement." *Biochimica et Biophysica Acta - Molecular Cell Research* 1404 (3): 271–81. https://doi.org/10.1016/S0167-4889(98)00080-9.

Song, Qinghe, Beibei Mao, Jinbo Cheng, Yuhao Gao, Ke Jiang, Jun Chen, Zengqiang Yuan, and Songshu Meng. 2015. "YAP Enhances Autophagic Flux to Promote Breast Cancer Cell Survival in Response to Nutrient Deprivation." *PLoS ONE* 10 (3). https://doi.org/10.1371/journal.pone.0120790.

Sotiropoulos, Athanassia, Dziugas Gineitis, John Copeland, and Richard Treisman. 1999. "Signal-Regulated Activation of Serum Response Factor Is Mediated by Changes in Actin Dynamics." *Cell* 98 (2): 159–69. https://doi.org/10.1016/S0092-8674(00)81011-9.

Speck, Samuel H, and Don Ganem. 2010. "Viral Latency and Its Regulation: Lessons from the γ-Herpesviruses." *Cell Host and Microbe* 8 (1): 100–115. https://doi.org/10.1016/j.chom.2010.06.014.

Staskus, K A, W Zhong, K Gebhard, B Herndier, H Wang, R Renne, J Beneke, et al. 1997. "Kaposi's Sarcoma-Associated Herpesvirus Gene Expression in Endothelial (Spindle) Tumor Cells." *Journal of Virology* 71 (1): 715–19. https://doi.org/10.1128/jvi.71.1.715-719.1997.

Stoecklin, Georg, Thomas Mayo, and Paul Anderson. 2006. "ARE-MRNA Degradation Requires

1158 the 5'-3' Decay Pathway." *EMBO Reports* 7 (1): 72–77.
1159 https://doi.org/10.1038/sj.embor.7400572.
1160 Sugimoto, Wataru, Katsuhiko Itoh, Yasumasa Mitsui, Takahiro Ebata, Hideaki Fujita, Hiroaki
1161 Hirata, and Keiko Kawauchi. 2018. "Substrate Rigidity-Dependent Positive Feedback
1162 Regulation between YAP and ROCK2." *Cell Adhesion and Migration* 12 (2): 101–8.
1163 https://doi.org/10.1080/19336918.2017.1338233.
1164 Takahashi, Shinya, Kyoko Sakurai, Arisa Ebihara, Hiroaki Kajiho, Kota Saito, Kenji Kontani,
1165 Hiroshi Nishina, and Toshiaki Katada. 2011. "RhoA Activation Participates in
1166 Rearrangement of Processing Bodies and Release of Nucleated AU-Rich MRNAs." *Nucleic*
1167 *Acids Research* 39 (8): 3446–57. https://doi.org/10.1093/nar/gkq1302.
1168 Tan, John L, Joe Tien, Dana M Pirone, Darren S Gray, Kiran Bhadriraju, and Christopher S
1169 Chen. 2003. "Cells Lying on a Bed of Microneedles: An Approach to Isolate Mechanical
1170 Force." *Proceedings of the National Academy of Sciences* 100 (4): 1484–89.
1171 https://doi.org/10.1073/pnas.0235407100.
1172 Tojkander, Sari, Gergana Gateva, and Pekka Lappalainen. 2012. "Actin Stress Fibers -
1173 Assembly, Dynamics and Biological Roles." *Journal of Cell Science* 125 (Pt 8): 1855–64.
1174 https://doi.org/10.1242/jcs.098087.
1175 Totaro, Antonio, Qiuyu Zhuang, Tito Panciera, Giusy Battilana, Luca Azzolin, Giulia Brumana,
1176 Alessandro Gandin, Giovanna Brusatin, Michelangelo Cordenonsi, and Stefano Piccolo.
1177 2019. "Cell Phenotypic Plasticity Requires Autophagic Flux Driven by YAP/TAZ
1178 Mechanotransduction." *Proceedings of the National Academy of Sciences* 116 (36): 17848–
1179 57. https://doi.org/10.1073/pnas.1908228116.
1180 Tutucci, Evelina, Maria Vera, Jeetayu Biswas, Jennifer Garcia, Roy Parker, and Robert H.
1181 Singer. 2018. "An Improved MS2 System for Accurate Reporting of the MRNA Life
1182 Cycle." *Nature Methods* 15 (1): 81–89. https://doi.org/10.1038/nmeth.4502.
1183 Umbach, Jennifer L, Hui Ling Yen, Leo L M Poon, and Bryan R Cullen. 2010. "Influenza a
1184 Virus Expresses High Levels of an Unusual Class of Small Viral Leader RNAs in Infected
1185 Cells." *MBio* 1 (4): 1–8. https://doi.org/10.1128/mBio.00204-10.
1186 Vallenius, Tea. 2013. "Actin Stress Fibre Subtypes in Mesenchymal-Migrating Cells." *Open*
1187 *Biology* 3 (6): 130001. https://doi.org/10.1098/rsob.130001.
1188 Vassilev, Alex, Kotaro J Kaneko, Hongjun Shu, Yingming Zhao, and Melvin L. DePamphilis.

2001. “TEAD/TEF Transcription Factors Utilize the Activation Domain of YAP65, a Src/Yes-Associated Protein Localized in the Cytoplasm.” *Genes and Development* 15 (10): 1229–41. https://doi.org/10.1101/gad.888601.

Vindry, Caroline, Aline Marnef, Helen Broomhead, Laure Twyffels, Sevim Ozgur, Georg Stoecklin, Miriam Llorian, et al. 2017. “Dual RNA Processing Roles of Pat1b via Cytoplasmic Lsm1-7 and Nuclear Lsm2-8 Complexes.” *Cell Reports* 20 (5): 1187–1200. https://doi.org/10.1016/j.celrep.2017.06.091.

Vozzi, Federico, Jonica Campolo, Lorena Cozzi, Gianfranco Politano, Stefano Di Carlo, Michela Rial, Claudio Domenici, and Oberdan Parodi. 2018. “Computing of Low Shear Stress-Driven Endothelial Gene Network Involved in Early Stages of Atherosclerotic Process.” *BioMed Research International* 2018 (September): 1–12. https://doi.org/10.1155/2018/5359830.

Wada, KI, K Itoga, T Okano, S Yonemura, and H Sasaki. 2011. “Hippo Pathway Regulation by Cell Morphology and Stress Fibers.” *Development* 138 (18): 3907–14. https://doi.org/10.1242/dev.070987.

Wakatsuki, T, B Schwab, N Thompson, and EL Elson. 2001. “Effects of Cytochalasin D and Latrunculin B on Mechanical Properties of Cells.” *Journal of Cell Science* 114 (5): 1025–36.

Wang, Huanru, Liang Chang, Xiaohui Wang, Airong Su, Chunhong Feng, Yuxuan Fu, Deyan Chen, Nan Zheng, and Zhiwei Wu. 2016. “MOV10 Interacts with Enterovirus 71 Genomic 5′UTR and Modulates Viral Replication.” *Biochemical and Biophysical Research Communications* 479 (3): 571–77. https://doi.org/10.1016/j.bbrc.2016.09.112.

Wang, Kuei-Chun, Yi-Ting Yeh, Phu Nguyen, Elaine Limqueco, Jocelyn Lopez, Satenick Thorossian, Kun-Liang Guan, Yi-Shuan J. Li, and Shu Chien. 2016. “Flow-Dependent YAP/TAZ Activities Regulate Endothelial Phenotypes and Atherosclerosis.” *Proceedings of the National Academy of Sciences* 113 (41): 11525–30. https://doi.org/10.1073/pnas.1613121113.

Wang, Xiaoli, Yingying Zhang, Tang Feng, Guanyue Su, Jia He, Wenbo Gao, Yang Shen, and Xiaoheng Liu. 2018. “Fluid Shear Stress Promotes Autophagy in Hepatocellular Carcinoma Cells.” *International Journal of Biological Sciences* 14 (10): 1277–90. https://doi.org/10.7150/ijbs.27055.

1220 Watanabe, Naoki, Takayuki Kato, Akiko Fujita, Toshimasa Ishizaki, and Shuh Narumiya. 1999.
1221 "Cooperation between MDia1 and ROCK in Rho-Induced Actin Reorganization." *Nature*
1222 *Cell Biology* 1 (3): 136–43. https://doi.org/10.1038/11056.
1223 Watanabe, Naoki, Pascal Madaule, Tim Reid, Toshimasa Ishizaki, Go Watanabe, Akira
1224 Kakizuka, Yuji Saito, Kazuwa Nakao, Brigitte M. Jockusch, and Shuh Narumiya. 1997.
1225 "P140mDia, a Mammalian Homolog of Drosophila Diaphanous, Is a Target Protein for Rho
1226 Small GTPase and Is a Ligand for Profilin." *EMBO Journal* 16 (11): 3044–56.
1227 https://doi.org/10.1093/emboj/16.11.3044.
1228 Wilbertz, Johannes H, Franka Voigt, Ivana Horvathova, Gregory Roth, Yinxiu Zhan, and Jeffrey
1229 A. Chao. 2019. "Single-Molecule Imaging of MRNA Localization and Regulation during
1230 the Integrated Stress Response." *Molecular Cell* 73 (5): 946-958.e7.
1231 https://doi.org/10.1016/j.molcel.2018.12.006.
1232 Winzen, Reinhard, Michael Kracht, Birgit Ritter, Arno Wilhelm, Chyi Ying A Chen, Ann Bin
1233 Shyu, Monika Müller, Matthias Gaestel, Klaus Resch, and Helmut Holtmann. 1999. "The
1234 P38 MAP Kinase Pathway Signals for Cytokine-Induced MRNA Stabilization via MAP
1235 Kinase-Activated Protein Kinase 2 and an AU-Rich Region-Targeted Mechanism." *EMBO*
1236 *Journal* 18 (18): 4969–80. https://doi.org/10.1093/emboj/18.18.4969.
1237 Yang, Chih-Sheng, Eleni Stampouloglou, Nathan M Kingston, Liye Zhang, Stefano Monti, and
1238 Xaralabos Varelas. 2018. "Glutamine-utilizing Transaminases Are a Metabolic
1239 Vulnerability of TAZ/YAP-activated Cancer Cells." *EMBO Reports* 19 (6): 1–11.
1240 https://doi.org/10.15252/embr.201643577.
1241 Yang, Ya Li, Lindsay M. Leone, and Laura J. Kaufman. 2009. "Elastic Moduli of Collagen Gels
1242 Can Be Predicted from Two-Dimensional Confocal Microscopy." *Biophysical Journal* 97
1243 (7): 2051–60. https://doi.org/10.1016/j.bpj.2009.07.035.
1244 Yao, Pingbo, Hong Zhao, Wenjuan Mo, and Pingping He. 2015. "Laminar Shear Stress
1245 Promotes Vascular Endothelial Cell Autophagy Through Upregulation with Rab4." *DNA*
1246 *and Cell Biology* 35 (3): 118–23. https://doi.org/10.1089/dna.2015.3041.
1247 Yu, Fa Xing, Bin Zhao, Nattapon Panupinthu, Jenna L. Jewell, Ian Lian, Lloyd H. Wang,
1248 Jiagang Zhao, et al. 2012. "Regulation of the Hippo-YAP Pathway by G-Protein-Coupled
1249 Receptor Signaling." *Cell* 150 (4): 780–91. https://doi.org/10.1016/j.cell.2012.06.037.
1250 Yu, Jiang Hong, Wei-Hong Yang, Tod Gulick, Kenneth D Bloch, and Donald B Bloch. 2005.

"Ge-1 Is a Central Component of the Mammalian Cytoplasmic MRNA Processing Body." *RNA (New York, N.Y.)* 11 (12): 1795–1802. https://doi.org/10.1261/rna.2142405.

Zanconato, Francesca, Mattia Forcato, Giusy Battilana, Luca Azzolin, Erika Quaranta, Beatrice Bodega, Antonio Rosato, Silvio Bicciato, Michelangelo Cordenonsi, and Stefano Piccolo. 2015. "Genome-Wide Association between YAP/TAZ/TEAD and AP-1 at Enhancers Drives Oncogenic Growth." *Nature Cell Biology* 17 (9): 1218–27. https://doi.org/10.1038/ncb3216.

Zhang, Qian, Fansen Meng, Shasha Chen, Steven W Plouffe, Shiying Wu, Shengduo Liu, Xinran Li, et al. 2017. "Hippo Signalling Governs Cytosolic Nucleic Acid Sensing through YAP / TAZ-Mediated TBK1 Blockade." *Nature Cell Biology* 19 (4): 362–74. https://doi.org/10.1038/ncb3496.

Zhao, Bin, Li Li, Lloyd Wang, Cun Yu Wang, Jindan Yu, and Kun Liang Guan. 2012. "Cell Detachment Activates the Hippo Pathway via Cytoskeleton Reorganization to Induce Anoikis." *Genes and Development* 26 (1): 54–68. https://doi.org/10.1101/gad.173435.111.

Zhao, Bin, Bin Zhao, Xiaomu Wei, Xiaomu Wei, Weiquan Li, Weiquan Li, Ryan S Udan, et al. 2007. "Inactivation of YAP Oncoprotein by the Hippo Pathway Is Involved in Cell Contact Inhibition and Tissue Growth Control." *Genes and Development* 21: 2747–61. https://doi.org/10.1101/gad.1602907.Hpo/Sav.

Zhong, W, H Wang, B Herndier, and D Ganem. 1996. "Restricted Expression of Kaposi Sarcoma-Associated Herpesvirus (Human Herpesvirus 8) Genes in Kaposi Sarcoma." *Proceedings of the National Academy of Sciences of the United States of America* 93 (13): 6641–46. https://doi.org/10.1073/pnas.93.13.6641.

Acknowledgements

We would like to sincerely thank the members of the Corcoran lab for helpful discussions about this work. We would like to thank Dr. Craig McCormick (Dalhousie University) for helpful discussions on this manuscript and his lab for plasmids, expertise and invaluable advice. ELC was supported by a Killam predoctoral scholarship, an NSERC CGS-M scholarship, and a Nova Scotia Graduate scholarship. Operating funds to support this work derive from an NSERC Discovery grant RGPIN-2015-04882 to JAC.

Competing Interests

The authors have no competing interests to declare.

1289 **Figure Legends**
1290

1291 **Figure 1: The RhoA-effector mDia1 is required for KapB-mediated PB disassembly.** KapB-
1292 and vector- expressing HUVECs were transduced with shRNAs targeting mDia1 (shDIA1-1,
1293 shDIA1-2) or with a non-targeting (shNT) control and selected. In parallel, cells were fixed for
1294 immunofluorescence or lysed for immunoblotting. (A) One representative immunoblot of three
1295 independent experiments stained with mDia1-specific antibody is shown. (B, C) Fixed cells were
1296 stained for CellProfiler analysis as detailed in the methods. (B) The number of EDC4 puncta per
1297 cell was quantified and normalized to the vector NT control within each replicate. (C)
1298 CellProfiler data was used to calculate the ratio of EDC4 puncta counts in KapB-expressing cells
1299 versus the vector control for each treatment condition. (D) Representative images of cells stained
1300 for PB-resident protein EDC4 (green), KapB (blue), and F-actin (red, phalloidin). Boxes indicate
1301 area shown in the EDC4 (zoom) panel. Scale bar represents 20 μm. Statistics were determined
1302 using ratio paired t-tests between control and experimental groups; error bars represent standard
1303 deviation; n=3 independent biological replicates; * = $p < 0.05$, ** = $p < 0.01$.
1304

1305 **Figure 2: The RhoA-effector ROCK is required for KapB-mediated PB disassembly.** (A-C)
1306 KapB- and vector- expressing HUVECs were treated with 10 ⌈M Y-27632 or water control for 4
1307 h and fixed for immunofluorescence. (A) Representative images of cells stained for PB-resident
1308 protein EDC4 (green), KapB (blue), and F-actin (red, phalloidin). Boxes indicate area shown in
1309 the EDC4 (zoom) panel. Scale bar represents 20 μm. (B, C) Fixed cells were stained for
1310 CellProfiler analysis as detailed in the methods. (B) The number of EDC4 puncta per cell was
1311 quantified and normalized to the vector NT control within each replicate. (C) CellProfiler data
1312 was used to calculate the ratio of EDC4 puncta counts in KapB-expressing cells versus the vector
1313 control for each treatment condition. (D-F) KapB- and vector- expressing HUVECs were
1314 transduced with shRNAs targeting ROCK1 and ROCK2 (shROCK1-1, shROCK1-2, shROCK2-
1315 1, shROCK2-2) or with a non-targeting (shNT) control and selected. Cells were fixed for
1316 immunofluorescence. (D, E) Fixed cells were stained for CellProfiler analysis as detailed in the
1317 methods. (D) The number of EDC4 puncta per cell was quantified and normalized to the vector
1318 NT control within each replicate. (E) CellProfiler data was used to calculate the ratio of EDC4
1319 puncta counts in KapB-expressing cells versus the vector control for each treatment condition.

1320 (F) Representative images of cells stained for PB-resident protein EDC4 (green), KapB (blue),
1321 and F-actin (red, phalloidin). Boxes indicate images shown in EDC4 (zoom) panel. Scale bar
1322 represents 20 μm. Statistics were determined using ratio paired t-tests between control and
1323 experimental groups; error bars represent standard deviation from n=3 independent biological
1324 replicates except shROCK1-2, (n=2); * = $p < 0.05$, ** = $p < 0.01$.
1325
1326 **Figure 3: Actomyosin contractility controls PB disassembly.** (A-C) KapB- and vector-
1327 expressing HUVECs were treated with 10 ⌈M blebbistatin to inhibit actomyosin contractility or
1328 DMSO for 30 min and fixed for immunofluorescence. (A, B) Fixed cells were stained for
1329 CellProfiler analysis as detailed in the methods. (A) The number of EDC4 puncta per cell was
1330 quantified and normalized to the vector NT control within each replicate. (B) CellProfiler data
1331 was used to calculate the ratio of EDC4 puncta counts in KapB-expressing cells versus the vector
1332 control for each treatment condition. (C) Representative images of cells stained for PB-resident
1333 protein EDC4 (green), KapB (blue), and F-actin (red, phalloidin). Boxes indicate area shown in
1334 the EDC4 (zoom) panel. Scale bar represents 20 μm. (D, E) Untransduced HUVECs were treated
1335 with 5 nM Calyculin A (CalA) to stimulate actomyosin contraction or DMSO for 20 min and
1336 fixed for immunofluorescence. (D) Fixed cells were stained for CellProfiler analysis as detailed
1337 in the methods. EDC4 puncta per cell were quantified and normalized to the DMSO control
1338 within each replicate. (E) Representative images of cells treated with 5 nM CalA and stained for
1339 PB-resident protein EDC4 (green) and F-actin (red, phalloidin). Boxes indicate area shown in the
1340 EDC4 (zoom) panel. Scale bar represents 20 μm. Statistics were determined using ratio paired t-
1341 tests between control and experimental groups; error bars represent standard deviation; n=3 (A,
1342 B) and n=5 (D) independent biological replicates; * = $p < 0.05$.
1343
1344 **Figure 4: YAP is required for KapB-mediated PB disassembly.** KapB- and vector-
1345 expressing HUVECs were transduced with shRNAs targeting YAP (shYAP-1, shYAP-2) or with
1346 a non-targeting (shNT) control and selected. In parallel, cells were fixed for immunofluorescence
1347 or lysed for immunoblotting. (A) One representative immunoblot of three independent
1348 experiments stained with YAP-specific antibody is shown. (B-D) Fixed cells were stained for
1349 CellProfiler analysis as detailed in the methods. (B) The number of EDC4 puncta per cell was
1350 quantified and normalized to the vector NT control within each replicate. (C) CellProfiler data

1351 was used to calculate the ratio of EDC4 puncta count in KapB-expressing cells to the vector
1352 control for each treatment condition. (D) Representative images of cells stained for PB-resident
1353 protein EDC4 (green), KapB (blue), and F-actin (red, phalloidin). Boxes indicate area shown in
1354 the EDC4 (zoom) panel. Scale bar represents 20 μm. Statistics were determined using ratio
1355 paired t-tests between control and experimental groups; error bars represent standard deviation;
1356 n=3 independent biological replicates; * = $p < 0.05$, ** = $p < 0.01$, *** = $p < 0.001$.
1357
1358 **Figure 5: Active YAP elicits PB disassembly.** (A, B, D-F) HUVECs were transduced with
1359 YAP 5SA-expressing and empty vector lentivirus and selected. Cells were fixed for
1360 immunofluorescence. (A) Representative images of cells stained for PB-resident protein EDC4
1361 (green) and F-actin (red, phalloidin). Boxes indicate area shown in the EDC4 (zoom) panel.
1362 Scale bar represents 20 μm. (B) Fixed cells were stained for CellProfiler analysis as detailed in
1363 the methods. The number of EDC4 puncta per cell was quantified and normalized to the vector
1364 control. (C) HeLa Tet-Off cells were seeded and co-transfected with an ARE-containing Firefly
1365 luciferase (Fluc) reporter plasmid, a Renilla luciferase (Rluc) reporter plasmid lacking an ARE,
1366 and either a KapB, YAP 5SA expression plasmid or vector controls. At 36 h post-transfection,
1367 transcription was terminated with doxycycline treatment for 12 h. Fluc and Rluc activity was
1368 measured. Data is normalized to vector control within each replicate. Graphs show the ratio of
1369 Fluc to Rluc, independent Fluc values and independent Rluc values, respectively. (D-F)
1370 Representative images of cells stained for (D) DDX6 (red), DCP1a (green) and DAPI (blue), (E)
1371 DDX6 (red), EDC4 (green) and DAPI (blue), and (D) DDX6 (red), YAP (green) and DAPI
1372 (blue). Boxes indicate area shown in the zoom panels. Scale bar represents 20 μm. Statistics
1373 were determined using ratio paired t-tests between control and experimental groups (B) or
1374 repeated measures ANOVA (C); error bars represent standard deviation; n=3 independent
1375 biological replicates; * = $p < 0.05$, ** = $p < 0.01$.
1376
1377 **Figure 6: YAP transcriptional activity is required for PB disassembly.** HUVECs were
1378 transduced with YAP 5SA-, YAP 6SA- or vector-expressing lentivirus and selected. Cells were
1379 fixed for immunofluorescence. (A) Representative images of cells stained for EDC4 (red),
1380 DDX6 (green) and DAPI (blue). Boxes indicate area shown in the zoom panels. Scale bar
1381 represents 20 μm. (B) Fixed cells were stained for CellProfiler analysis as detailed in the

1382 methods. CellProfiler was used to count nuclei, EDC4 puncta and DDX6 puncta. In RStudio
1383 analysis, puncta with ≥ 60% correlation (mean correlation in vector control) between EDC4 and
1384 DDX6 (PBs) were counted and normalized to number of nuclei per condition. PB counts were
1385 normalized to vector control within each replicate.
1386
1387 **Figure 7: YAP Inputs Mediate PB Disassembly.** (A, B) HUVECs were seeded onto collagen-
1388 coated microscope slides and exposed to shear stress of 2 dyn/cm^2, 10 dyn/cm^2 or no shear (static
1389 control) for 21 h. Cells were fixed and stained for immunofluorescence. (A) Representative
1390 images of cells stained for PB-resident proteins EDC4 (green) and DDX6 (blue), as well as F-
1391 actin (red, phalloidin). Boxes indicate area shown in EDC4 (zoom) and DDX6 (zoom) panels.
1392 Scale bar represents 20 μm. (B) CellProfiler was used to count nuclei, EDC4 puncta and DDX6
1393 puncta. In RStudio analysis, puncta with ≥ 70% correlation (mean correlation in vector control)
1394 between EDC4 and DDX6 (PBs) were counted and normalized to number of nuclei per
1395 condition. PB counts were normalized to static control within each replicate. (C, D) HUVECs
1396 were split and seeded at a high-, medium- and low-density, cultured for 48 h and fixed for
1397 immunofluorescence. (C) Representative images of cells stained for the PB-resident protein
1398 EDC4 (green) and F-actin (red, phalloidin). Boxes indicate images shown in EDC4 (zoom)
1399 panel. Scale bar represents 20 μm. (D) Fixed cells were stained for CellProfiler analysis as
1400 detailed in the methods. The number of EDC4 puncta per cell was quantified and normalized to
1401 the high confluence condition. (E, F) Coverslips were coated for 4 h with 0 to 64 μg/cm^2 of
1402 collagen. HUVECs were grown for 72 h on coated coverslips and fixed for immunofluorescence.
1403 (E) Representative images of cells stained for PB-resident protein EDC4 (green), DDX6 (blue)
1404 and F-actin (red, phalloidin). Boxes indicate images shown in EDC4 (zoom) panel. Scale bar
1405 represents 20 μm. (F) Fixed cells were stained for CellProfiler analysis as detailed in the
1406 methods. The number of EDC4 puncta per cell was quantified and normalized to the 0 μg/mL
1407 collagen-coating condition. Statistics were determined using repeated measures ANOVA (A, B)
1408 or Pearson's correlation co-efficient (C); error bars represent standard deviation (A, B) and 95%
1409 confidence interval of line of best fit (slope is significantly non-zero, $p = 0.014$) (C); n=3
1410 independent biological replicates; * = $p < 0.05$, ** = $p < 0.01$.
1411

1412 **Figure 8: YAP is required for EDC4 puncta disassembly in HUVECs subjected to shear**
1413 **stress.** (A) HUVECs were seeded onto collagen-coated microscope slides and exposed to shear
1414 stress of 2 dyn/cm^2, 10 dyn/cm^2 or a static control for 21 h. Cells were lysed for immunoblotting.
1415 One representative immunoblot and quantification of three independent experiments stained with
1416 P(S127)-YAP- and YAP-specific antibody is shown. P(S127)-YAP and YAP protein levels in
1417 each condition were normalized to total protein. All treatments were normalized to static control
1418 within each replicate. (B, C) HUVECs were transduced with shRNAs targeting YAP (shYAP-2)
1419 or with a non-targeting (shNT) control and selected. Cells were seeded onto collagen-coated
1420 microscope slides and exposed to shear stress of 10 dyn/cm^2 or no shear (static control) for 21 h.
1421 Cells were fixed and stained for immunofluorescence. (B) CellProfiler was used to count nuclei
1422 and EDC4 puncta. In RStudio analysis, EDC4 puncta were normalized to number of nuclei per
1423 condition. EDC4 puncta counts were normalized to static control. (C) Representative images of
1424 cells stained for PB-resident protein EDC4 (red), DDX6 (green) and DAPI (blue). In parallel,
1425 separate coverslips were stained for F-actin (phalloidin). Boxes indicate area shown in the EDC4
1426 (zoom) panel. Scale bar represents 20 μm. Statistics were determined using repeated measures
1427 ANOVA (A); error bars represent standard deviation (A) ; n=4, except 2 dyn/cm^2 (n=3) (A) and
1428 n = 2 (B, C) independent biological replicates; * = $p < 0.05$, ** = $p < 0.01$.
1429

1430 **Figure 9: KapB activates a mechanoresponsive pathway from within the cell rather than**
1431 **without to mediate PB disassembly.** (A) Cells respond to external mechanical force by
1432 activating their structural support network, the actin cytoskeleton. The GTPase RhoA and its
1433 downstream effectors coordinate this response, bundling actin filaments into stress fibers (SFs),
1434 enhancing actomyosin contractility and increasing adhesion to the underlying matrix to help
1435 withstand force-induced membrane deformation. Together, these actin-based responses increase
1436 cytoskeletal tension and elicit the dephosphorylation and nuclear translocation of the
1437 mechanoresponsive transcription activator YAP where it collaborates with other transcription
1438 factors to induce TEAD-responsive genes. We present data to support the existence of a
1439 mechanoresponsive pathway that links actin SFs, actomyosin contractility, and the transcription
1440 transactivator YAP to the disassembly of PBs. The viral protein KapB taps into this
1441 mechanoresponsive pathway, triggering mechanical changes and forming contractile cytoskeletal
1442 structures that would normally respond to force, thereby inducing PB disassembly in a YAP-

1443 dependent manner, from within the cell, rather than from without. Both KapB and stimuli that
1444 activate YAP cause PB disassembly. (B) Both KapB and active YAP have been shown to
1445 upregulate autophagic flux (Robinson et al. 2021; Pavel et al. 2018); however, YAP 5SA also
1446 accelerates autophagosome-lysosome fusion by upregulating the Rab7-GTPase activating
1447 protein, Armus, while KapB does not increase Armus transcription. In our model, upregulated
1448 autophagic flux contributes PB disassembly mediated by both YAP 5SA and KapB.
1449
1450 **Figure S1: The RhoA-effector ROCK is required for KapB-mediated PB disassembly,**
1451 **knockdown confirmation and vector data.** (A) KapB- and vector- expressing HUVECs were
1452 treated with 10 μM Y-27632 or water control for 4 h and fixed for immunofluorescence. Fixed
1453 cells were stained for CellProfiler analysis as detailed in the methods. The number of EDC4
1454 puncta per cell was quantified and normalized to the vector control. Vector control data is
1455 shown. (B, C) KapB- and vector- expressing HUVECs were transduced with shRNAs targeting
1456 ROCK1 and ROCK2 (shROCK1-1, shROCK1-2, shROCK2-1, shROCK2-2) or with a non-
1457 targeting (shNT) control and selected. In parallel, cells were lysed for immunoblotting or fixed
1458 for immunofluorescence. (B) One representative immunoblot of three independent experiments
1459 stained using ROCK1- and 2-specific antibodies. (C) Fixed cells were stained for CellProfiler
1460 analysis as detailed in the methods. The number of EDC4 puncta per cell was quantified and
1461 normalized to the vector NT control within each replicate. Vector control data is shown.
1462 Statistics were determined using a ratio paired t-test between control and experimental groups;
1463 error bars represent standard deviation; n=3 independent biological replicates; * = $p < 0.05$.
1464
1465 **Figure S2: Cofilin knockdown augments KapB-mediated PB disassembly.** KapB- and
1466 vector- expressing HUVECs were transduced with shRNAs targeting cofilin (shCFN-1, shCFN-
1467 2) or with a non-targeting (shNT) control and selected. In parallel, cells were fixed for
1468 immunofluorescence or lysed for immunoblotting. (A) One representative immunoblot of three
1469 independent experiments stained using a cofilin-specific antibody. (B, C) Fixed cells were
1470 stained for CellProfiler analysis as detailed in the methods. (B) The number of EDC4 puncta per
1471 cell was quantified and normalized to the vector NT control within each replicate. (C)
1472 CellProfiler data was used to calculate the ratio of EDC4 puncta counts in KapB-expressing cells
1473 versus the vector control for each treatment condition. (D) Representative images of cells stained

1474 for PB-resident protein EDC4 (green), KapB (blue), and F-actin (red, phalloidin). Boxes indicate
1475 the area of the field of view that is shown in EDC4 (zoom) panel. Scale bar represents 20 μm.
1476 Statistics were determined using a ratio paired t-test between control and experimental groups;
1477 error bars represent standard deviation; n=3 independent biological replicates; * = $p < 0.05$.
1478
1479 **Figure S3: G-actin concentration does not control PB disassembly.** (A, B, C) HUVECs were
1480 treated with 1 μM Jasp (polymerizes actin and decreases monomeric G-actin), 1 μg/μL CytD
1481 (actin depolymerization to increase monomeric G-actin) or a DMSO control for 30 min. (A, B)
1482 Fixed cells were stained for CellProfiler analysis as detailed in the methods. The number of
1483 EDC4 puncta per cell was quantified and normalized to the DMSO control. (C) Representative
1484 images of cells stained for PB-resident protein EDC4 and F-actin (phalloidin). Actin is not seen
1485 in Jasp panel due to Jasp-mediated interference with phalloidin staining (Bubb et al. 1999). Scale
1486 bar represents 20 μm. Statistics were determined using a ratio paired t-test between control and
1487 experimental groups; error bars represent standard deviation; n=3 independent biological
1488 replicates. (D) Representative immunoblot of filamentous and globular actin fractions separated
1489 by ultracentrifugation as detailed in the methods from HUVECs treated with DMSO, 0.5 or 1.0
1490 μM Jasp. * = $p < 0.05$, ** = $p < 0.01$.
1491
1492 **Figure S4: α-actinin-1-overexpression mediated SF formation and PB disassembly.**
1493 HUVECs were fixed and stained with antibodies for (A) α-actinin-1 and (B) α-actinin-4. (C, D)
1494 HUVECs transduced with recombinant lentiviruses expressing GFP-tagged α-actinin-1 (ACTN-
1495 GFP) or a GFP control were selected and fixed for immunofluorescence. (C) Fixed cells were
1496 stained for CellProfiler analysis as detailed in the methods. The number of EDC4 puncta per cell
1497 was quantified and normalized to the vector GFP control. (D) Representative images of cells
1498 stained for PB-resident protein EDC4 (false-coloured green), ACTN-GFP (false-coloured blue),
1499 and F-actin (red, phalloidin). Boxes indicate images shown in EDC4 (zoom) panel. Scale bar
1500 represents 20 μm. Statistics were determined using a ratio paired t-test between control and
1501 experimental groups; error bars represent standard deviation; n=3 independent biological
1502 replicates; * = $p < 0.05$.
1503

1504 **Figure S5: KapB does not activate canonical functions of YAP.** (A, B) KapB- and vector-
1505 expressing HUVECs were lysed for immunoblotting or fixed for immunofluorescence. (A)
1506 Representative immunoblots and quantification of immunoblotting for P(S127)-YAP-, YAP- or
1507 KapB-specific antibody are shown. Several immunoblots are shown to illustrate variation in
1508 KapB-mediated changes in P-YAP and YAP. Protein levels in each condition were normalized to
1509 total protein. All treatments were normalized to vector control within each replicate. (B)
1510 Representative images of cells stained for YAP. Scale bar represents 20 μM. (C) HEK-293A
1511 cells were co-transfected with a firefly luciferase (Fluc) reporter plasmid with a YAP-responsive
1512 TEAD promoter element, a TREX-renilla luciferase (Rluc) reporter plasmid, and overexpression
1513 constructs for either a KapB, YAP 5SA or vector control. At 36 h post-transfection, cells were
1514 starved in serum-free DMEM for 12 h, lysed and Fluc and Rluc activity was recorded. Data is
1515 normalized to vector control. Graphs show the ratio of Fluc to Rluc, independent Fluc values and
1516 independent Rluc values, respectively. (D) HUVECs were transduced with recombinant
1517 lentiviruses expressing KapB, a constitutively active version of YAP (YAP 5SA) or an empty
1518 vector control, selected and lysed for total RNA. qRT-PCR analysis of steady state mRNA levels
1519 of canonical YAP-regulated genes CTGF, ANKRD1 and CYR61 was performed, and was
1520 normalized to steady state HPRT-1 mRNA levels. Statistics were determined using repeated
1521 measures ANOVA; error bars represent standard deviation; n=3 independent biological
1522 replicates; * = $p < 0.05$, ** = $p < 0.01$.
1523
1524 **Figure S6: YAP 5SA-mediated PB disassembly is not dependent on autophagy.** YAP 5SA-
1525 and vector- expressing HUVECs were treated with 10 nM BafA1 or DMSO control for 30 min
1526 and fixed for immunofluorescence. (A,B) Fixed cells were stained for LC3 puncta analysis as
1527 detailed in the methods. (A) Representative images of cells stained for LC3 (white) and DAPI
1528 (blue). Boxes indicate the area of the field of view that is shown in LC3 (zoom) panel. Scale bar
1529 represents 20 μm. (B) The number of LC3 puncta per cell was quantified in each condition.
1530 (C,D) Fixed cells were stained for CellProfiler analysis as detailed in the methods. (C)
1531 Representative images of cells stained for DDX6 (red), YAP (green) and DAPI (blue). Boxes
1532 indicate the area of the field of view that is shown in DDX6 (zoom) panel. Scale bar represents
1533 20 μm. (D) The number of DDX6 puncta per cell was quantified and normalized to the vector
1534 control within each replicate. (E) HUVECs were transduced with recombinant lentiviruses

1535 expressing KapB, a constitutively active version of YAP (YAP 5SA) or an empty vector control,
1536 selected and lysed for total RNA. qRT-PCR analysis of steady-state mRNA levels of the Rab7-
1537 GTPase activating protein, Armus, was performed, and was normalized to steady state HPRT-1
1538 mRNA levels. Statistics were determined using a two-way ANOVA with multiple comparisons
1539 between control and experimental groups; error bars represent standard deviation; n=3
1540 independent biological replicates; ** = $p < 0.01$, *** = $p<0.001$.
1541
1542
1543

1544 **Supplementary Files**

1545 **Supplementary File 1:** Table detailing antibodies used in this study, including species, target,
1546 source, use and dilution.

1547

1548 **Supplementary File 2:** Table detailing plasmids used in this study, including name, use, source,
1549 bacterial selection cassette and mammalian selection cassette.

1550

1551 **Supplementary File 3:** Table detailing shRNA sequences used in this study.

1552

1553 **Supplementary File 4:** Table detailing drug treatments used in this study, including name, use,
1554 source, concentration and duration of treatment.

1555

1556 **Supplementary File 5:** Table detailing qRT-PCR primers used in this study, including target,
1557 sequence, melting temperature, and reference.

1558

1559 **Source Code**

1560 **Source Code 1**: CellProfiler pipeline used to enumerate puncta from epifluorescent microscopy
1561 images of HUVECs stained for Hedls puncta; co-stained with DAPI and WGA.

1562

1563 **Source Code 2**: CellProfiler pipeline used to enumerate puncta from confocal microscopy
1564 images of HUVECs subjected to shear stress stained for Hedls and DDX6 puncta.

1565

1566 **Source Code 3**: CellProfiler pipeline used to enumerate puncta from confocal microscopy
1567 images of HUVECs subjected to shear stress stained for Hedls puncta.

1568

1569 **Source Code 4**: CellProfiler pipeline used to quantify intensity in nucleus and cytoplasm from
1570 epifluorescent microscopy images of HUVECs stained for YAP protein; co-stained with DAPI
1571 and WGA.

1572

1573 **Source Code 5**: CellProfiler pipeline used to enumerate puncta from epifluorescent microscopy
1574 images of HUVECs stained for LC3 puncta; co-stained with DAPI.

Source Code 6: Template RStudio code used for analysis of CellProfiler output from Source Code 1. Annotations provided within code.

Source Code 7: Template RStudio code used for analysis of CellProfiler output from Source Code 2. Annotations provided within code.

Source Code 8: Template RStudio code used for analysis of CellProfiler output from Source Code 3. Annotations provided within code.

Source Code 9: Template RStudio code used for analysis of CellProfiler output from Source Code 4. Annotations provided within code.

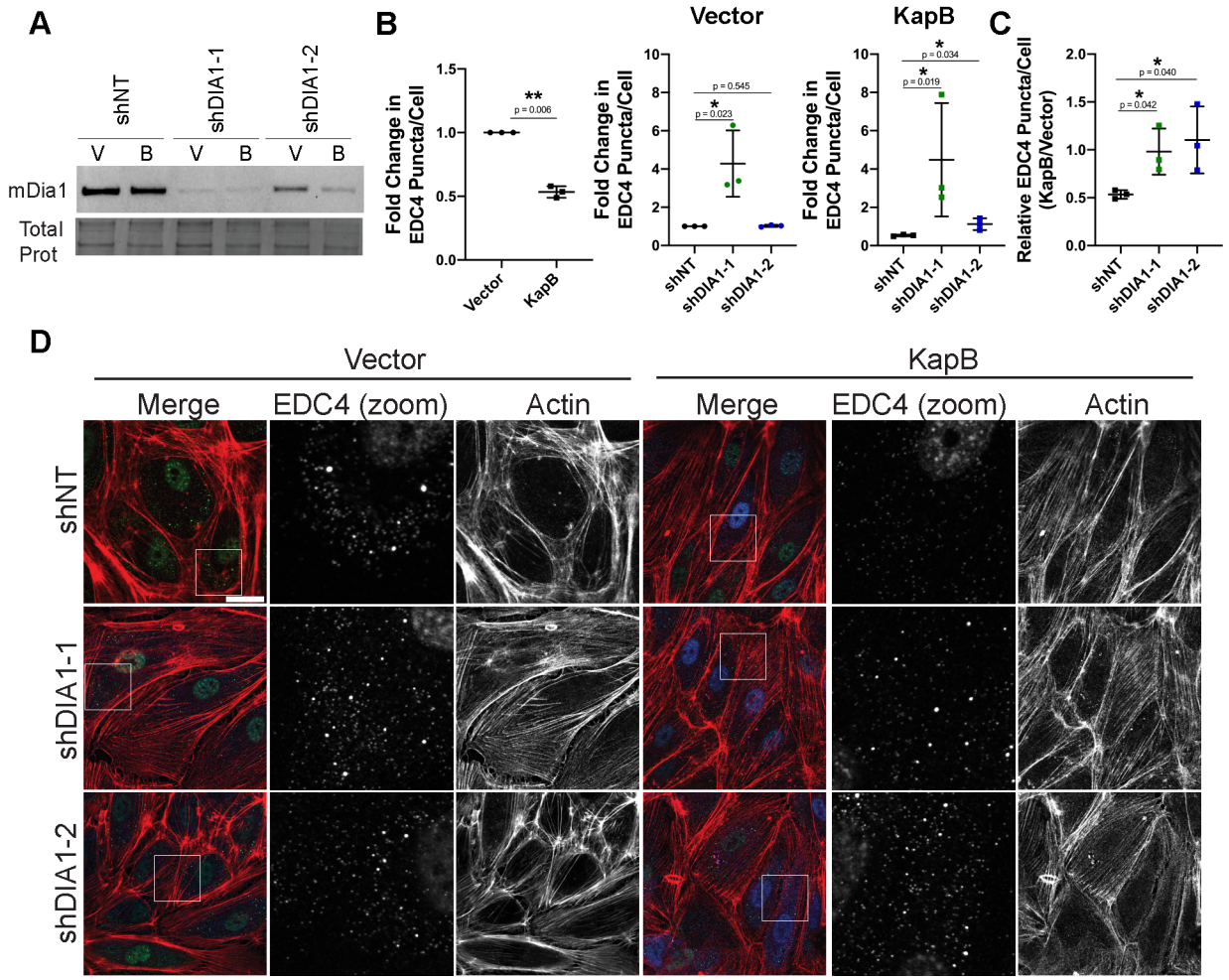
A
shNT
shDIA1-1
shDIA1-2
V B V B V B
mDia1
Total Prot
B
Vector
KapB
Fold Change in EDC4 Puncta/Cell
p = 0.006
p = 0.023
p = 0.545
p = 0.019
p = 0.034
Vector
KapB
shNT
shDIA1-1
shDIA1-2
C
Relative EDC4 Puncta/Cell (KapB/Vector)
p = 0.042
p = 0.040
D
Vector
KapB
Merge
EDC4 (zoom)
Actin
shNT
shDIA1-1
shDIA1-2

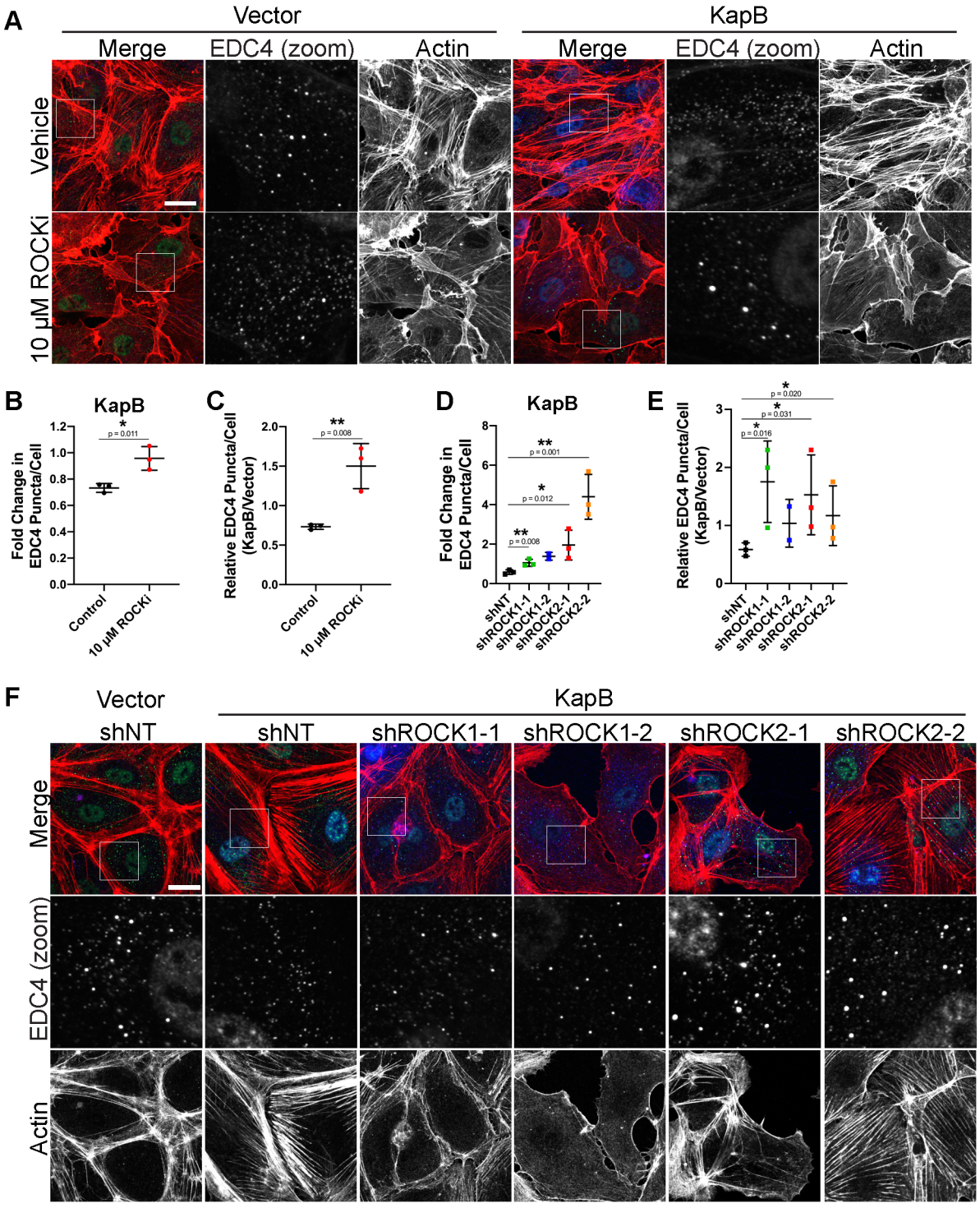
A
Vector
KapB
Merge
EDC4 (zoom)
Actin
Vehicle
10 μM ROCKi
B
KapB
Fold Change in EDC4 Puncta/Cell
p = 0.011
Control
10 μM ROCKi
C
Relative EDC4 Puncta/Cell (KapB/Vector)
p = 0.008
D
KapB
Fold Change in EDC4 Puncta/Cell
p = 0.008
p = 0.012
p = 0.001
shNT
shROCK1-1
shROCK1-2
shROCK2-1
shROCK2-2
E
Relative EDC4 Puncta/Cell (KapB/Vector)
p = 0.016
p = 0.031
p = 0.020
F
Vector
shNT
KapB
Merge
EDC4 (zoom)
Actin

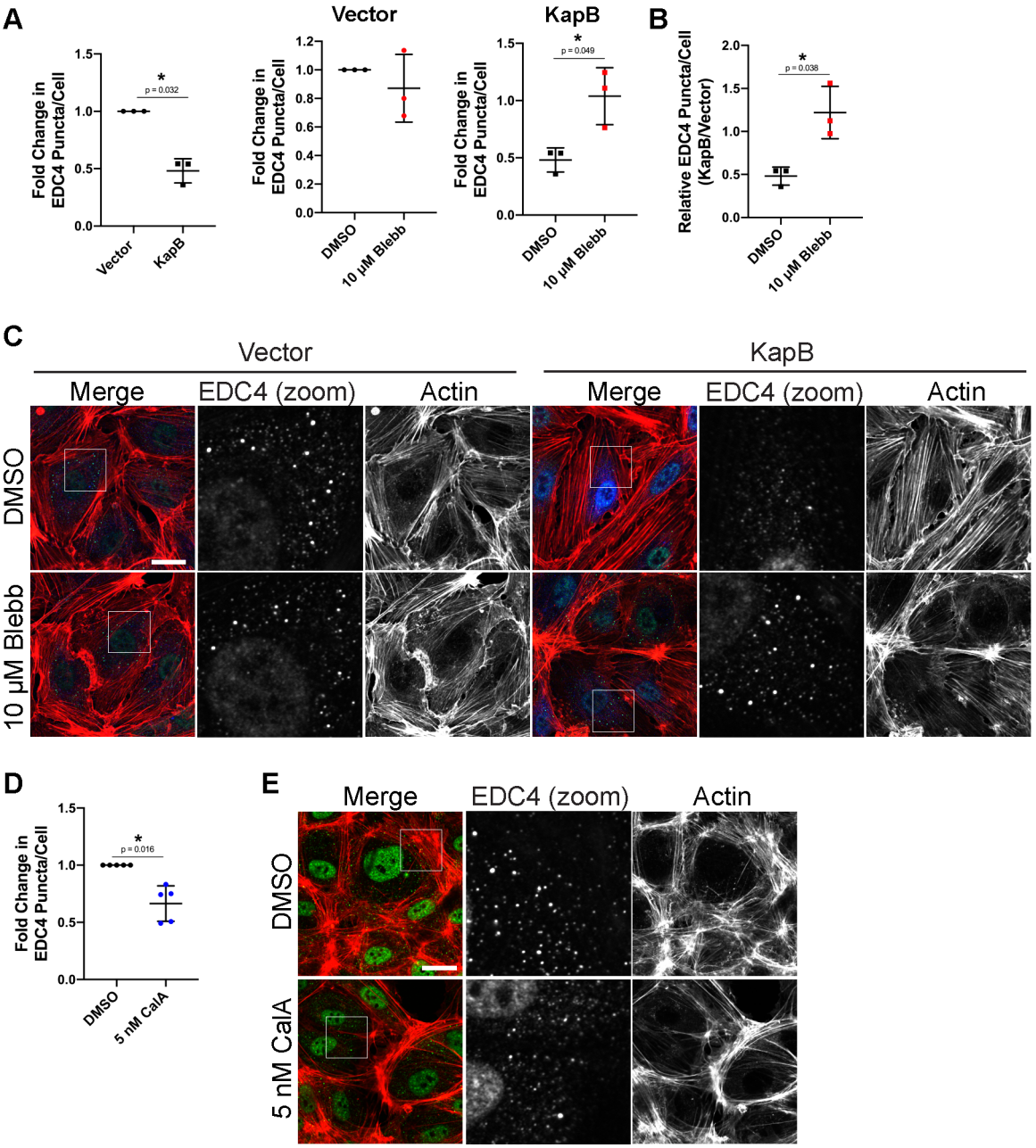
A
Vector
KapB
B
Fold Change in EDC4 Puncta/Cell
Relative EDC4 Puncta/Cell (KapB/Vector)
p = 0.032
p = 0.049
p = 0.038
Vector
KapB
DMSO
10 μM Blebb
C
Vector
KapB
Merge
EDC4 (zoom)
Actin
DMSO
10 μM Blebb
D
p = 0.016
DMSO
5 nM CalA
E
Merge
EDC4 (zoom)
Actin
DMSO
5 nM CalA

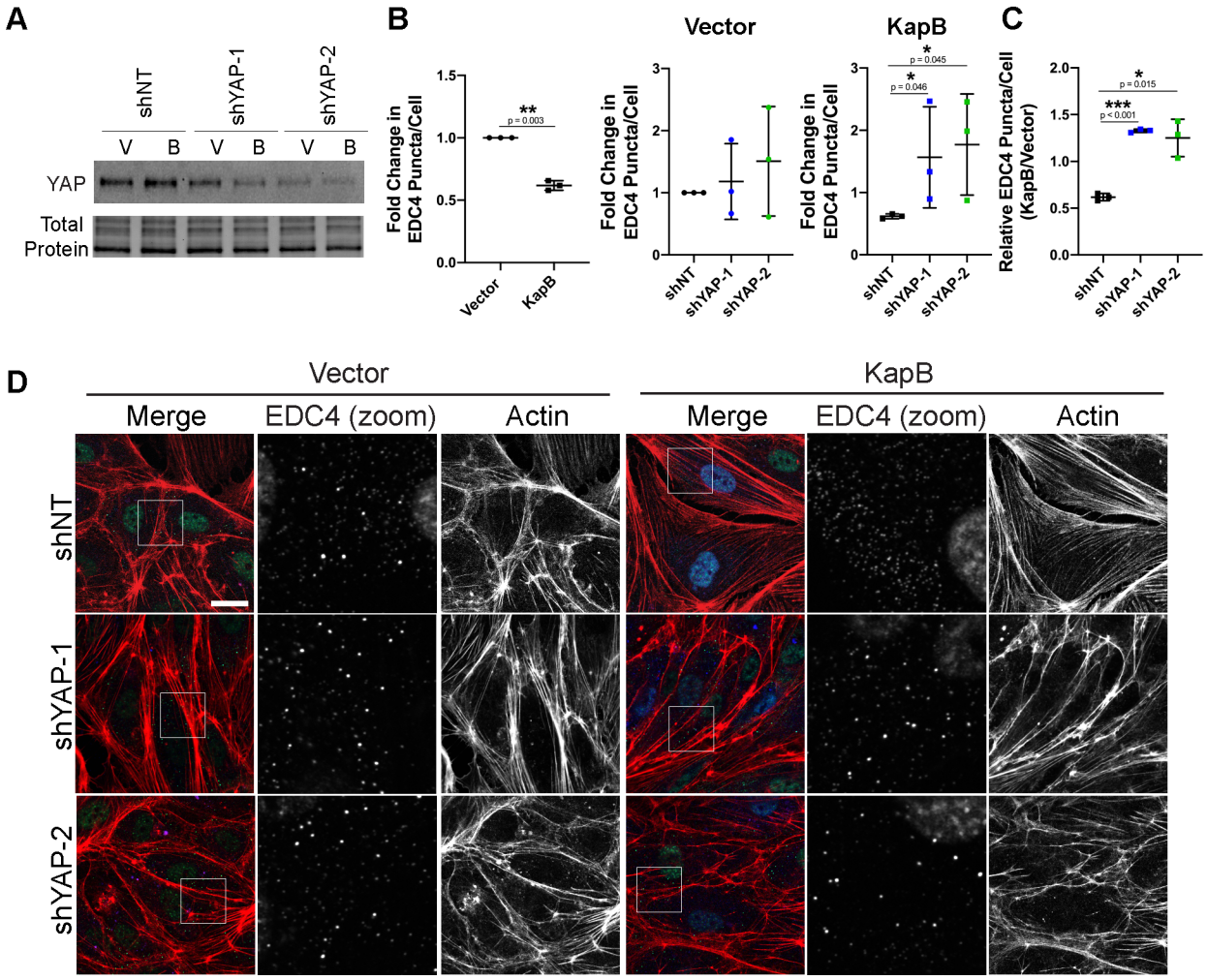
A
shNT
shYAP-1
shYAP-2
V B V B V B
YAP
Total Protein
B
Fold Change in EDC4 Puncta/Cell
**
p = 0.003
Vector
KapB
Vector
KapB
*
p = 0.045
*
p = 0.046
shNT
shYAP-1
shYAP-2
C
Relative EDC4 Puncta/Cell (KapB/Vector)
*
p = 0.015
***
p < 0.001
D
Vector
KapB
Merge
EDC4 (zoom)
Actin
shNT
shYAP-1
shYAP-2

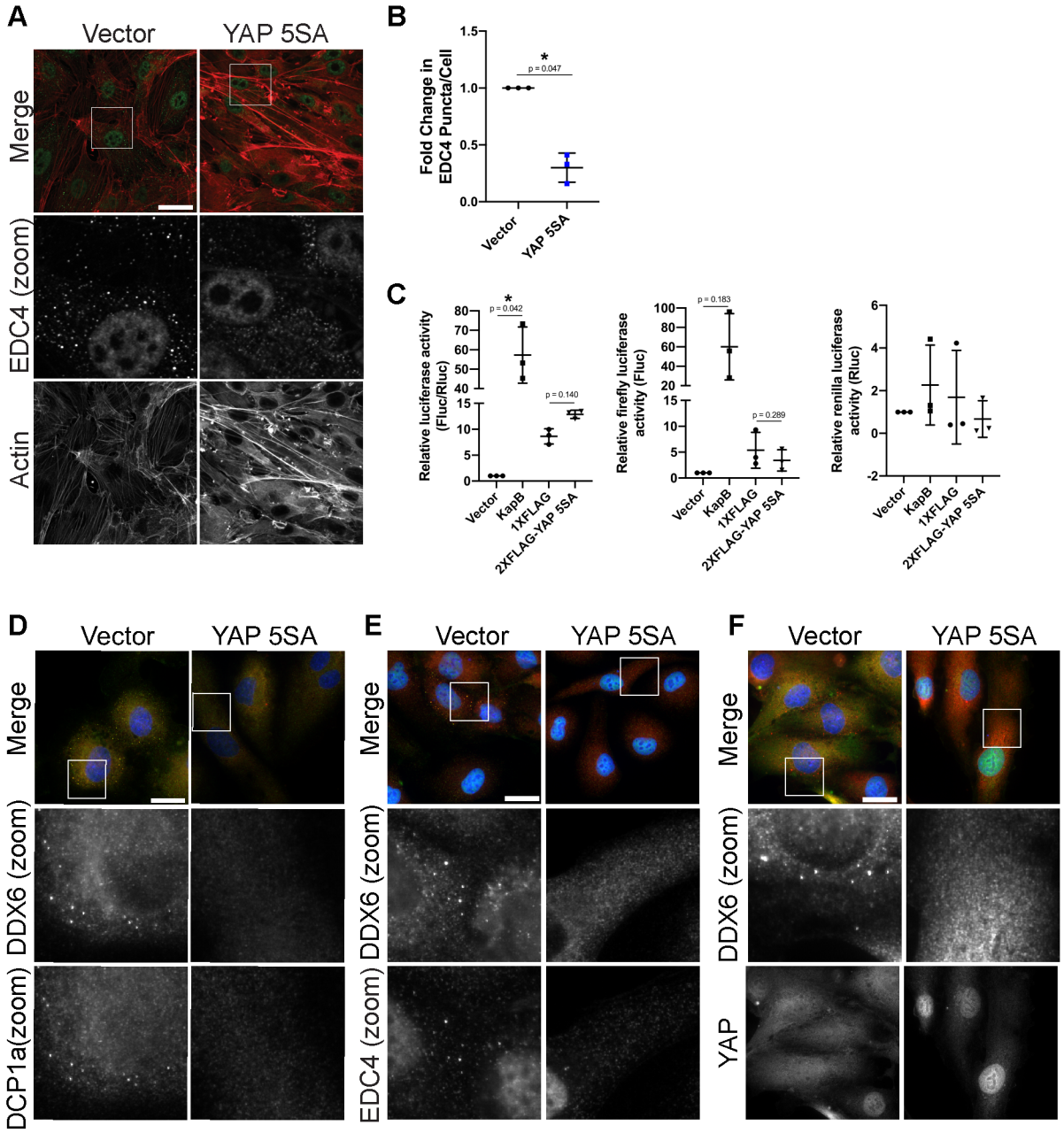
A
Vector
YAP 5SA
Merge
EDC4 (zoom)
Actin
B
Fold Change in EDC4 Puncta/Cell
1.5
1.0
0.5
0.0
*
p = 0.047
Vector
YAP 5SA
C
Relative luciferase activity (Fluc/Rluc)
80
70
60
50
40
15
10
5
0
*
p = 0.042
p = 0.140
Vector
KapB
1XFLAG
2XFLAG-YAP 5SA
Relative firefly luciferase activity (Fluc)
100
80
60
40
20
15
10
5
0
p = 0.183
p = 0.289
Vector
KapB
1XFLAG
2XFLAG-YAP 5SA
Relative renilla luciferase activity (Rluc)
6
4
2
0
-2
Vector
KapB
1XFLAG
2XFLAG-YAP 5SA
D
Vector
YAP 5SA
Merge
DDX6 (zoom)
DCP1a(zoom)
E
Vector
YAP 5SA
Merge
DDX6 (zoom)
EDC4 (zoom)
F
Vector
YAP 5SA
Merge
DDX6 (zoom)
YAP

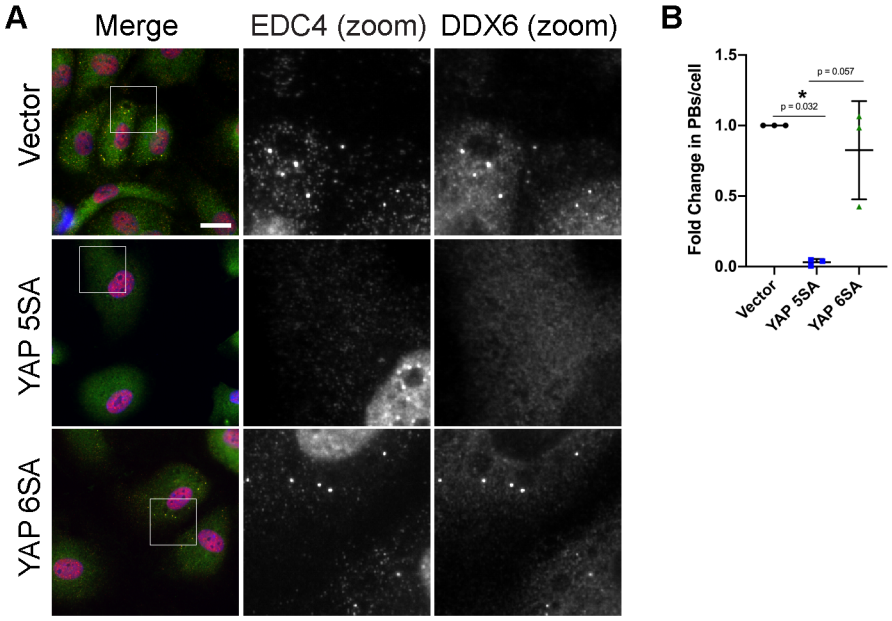
A
Merge
EDC4 (zoom)
DDX6 (zoom)
Vector
YAP 5SA
YAP 6SA
B
Fold Change in PBs/cell
1.5
1.0
0.5
0.0
p = 0.057
*
p = 0.032
Vector
YAP 5SA
YAP 6SA

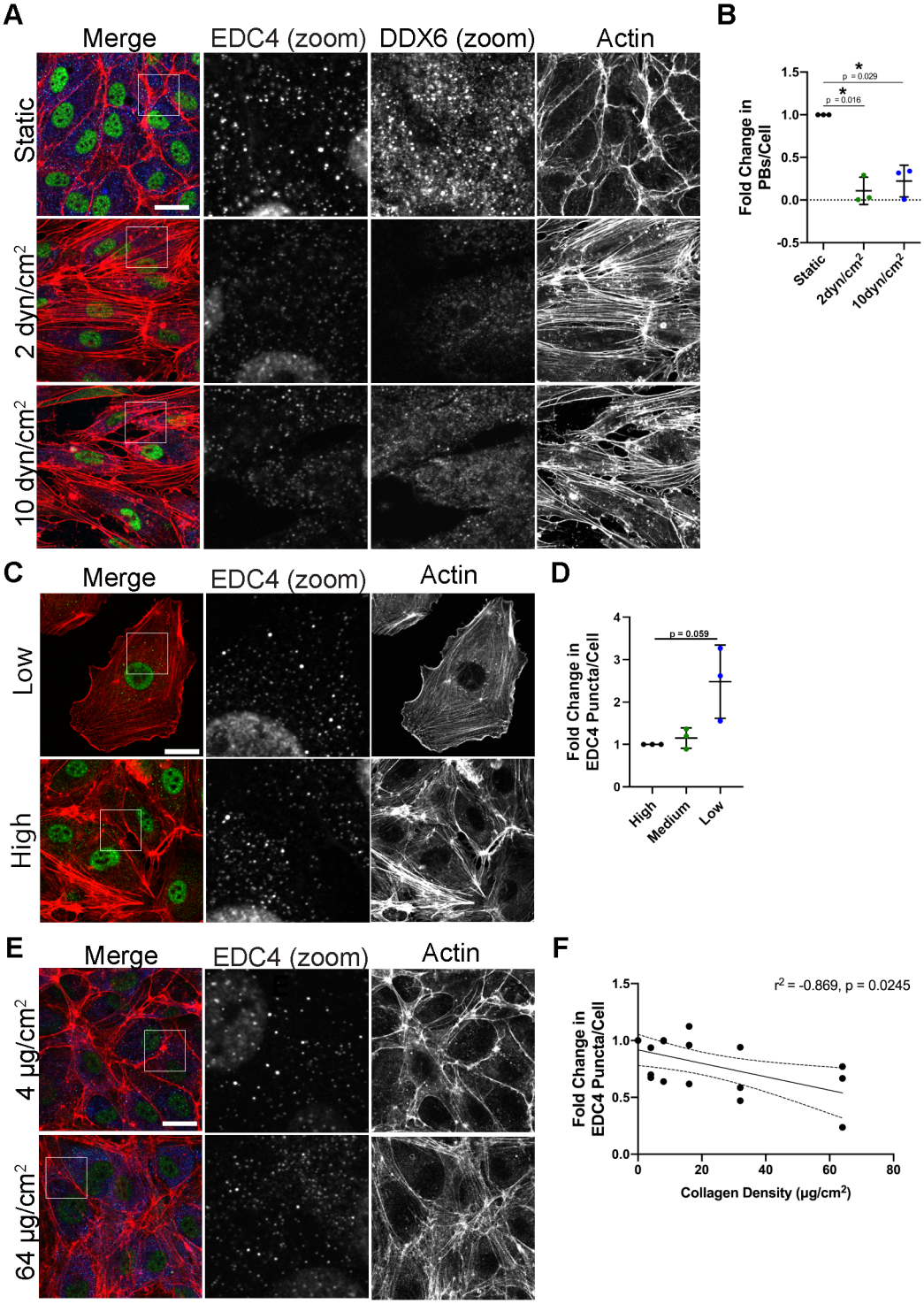
A
Merge
EDC4 (zoom)
DDX6 (zoom)
Actin
Static
2 dyn/cm2
10 dyn/cm2
B
Fold Change in PBs/Cell
p = 0.029
p = 0.016
Static
2dyn/cm2
10dyn/cm2
C
Merge
EDC4 (zoom)
Actin
Low
High
D
Fold Change in EDC4 Puncta/Cell
p = 0.059
High
Medium
Low
E
Merge
EDC4 (zoom)
Actin
4 µg/cm2
64 µg/cm2
F
r2 = -0.869, p = 0.0245
Fold Change in EDC4 Puncta/Cell
Collagen Density (µg/cm2)

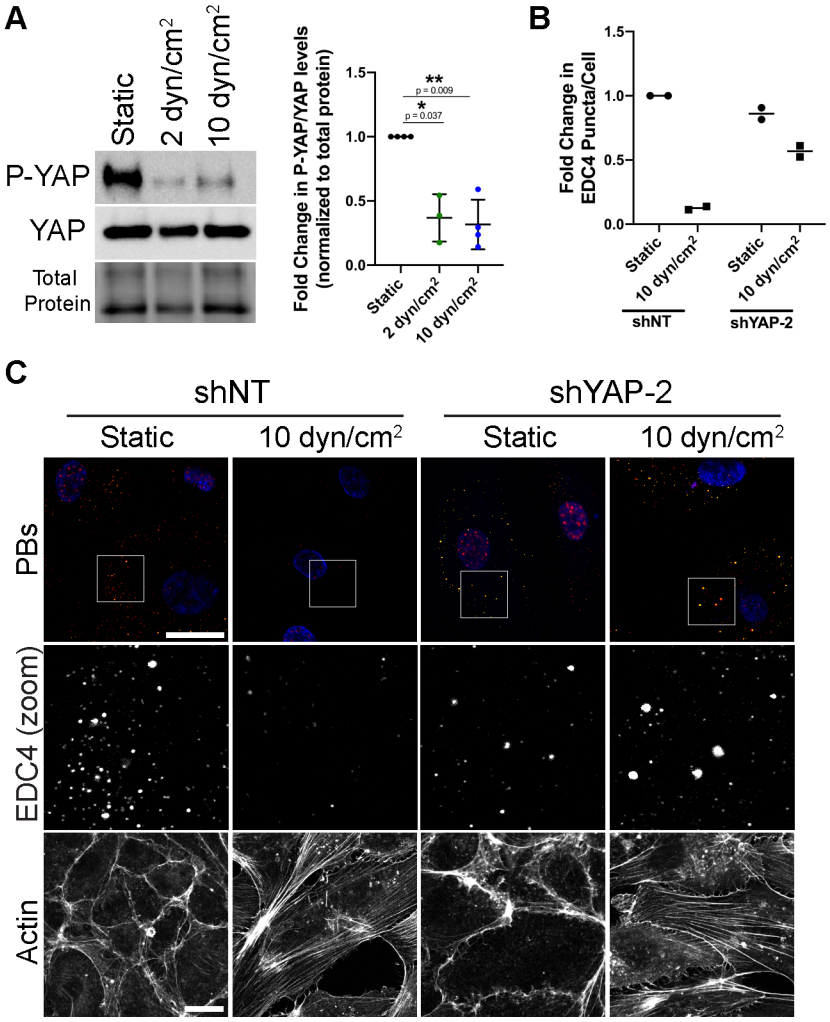
A
Static
2 dyn/cm2
10 dyn/cm2
P-YAP
YAP
Total Protein
Fold Change in P-YAP/YAP levels (normalized to total protein)
1.5
1.0
0.5
0.0
**
p = 0.009
*
p = 0.037
Static
2 dyn/cm2
10 dyn/cm2
B
Fold Change in EDC4 Puncta/Cell
1.5
1.0
0.5
0.0
Static
10 dyn/cm2
Static
10 dyn/cm2
shNT
shYAP-2
C
shNT
shYAP-2
Static
10 dyn/cm2
Static
10 dyn/cm2
PBs
EDC4 (zoom)
Actin

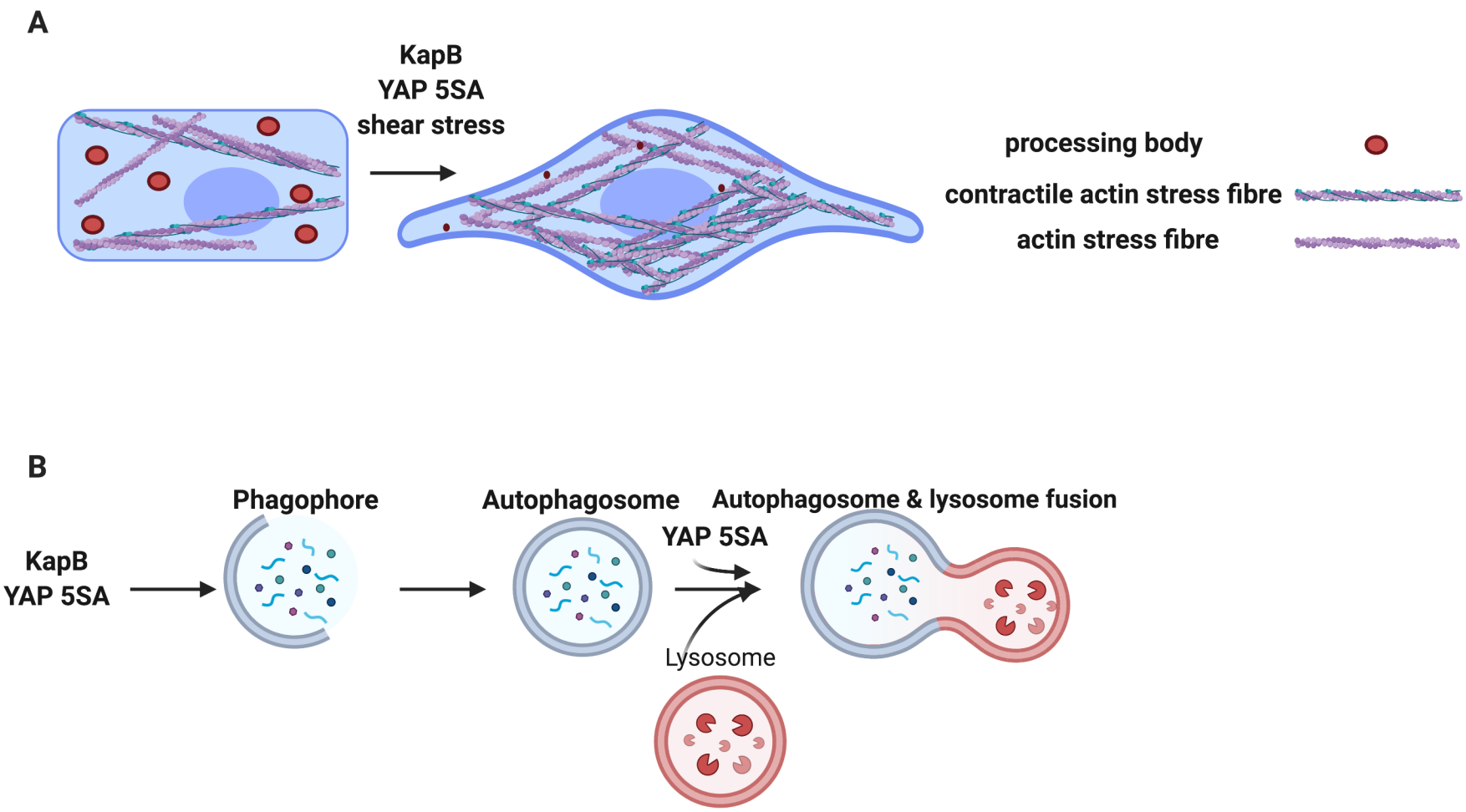
A
KapB
YAP 5SA
shear stress
processing body
contractile actin stress fibre
actin stress fibre
B
KapB
YAP 5SA
Phagophore
Autophagosome
Autophagosome & lysosome fusion
YAP 5SA
Lysosome

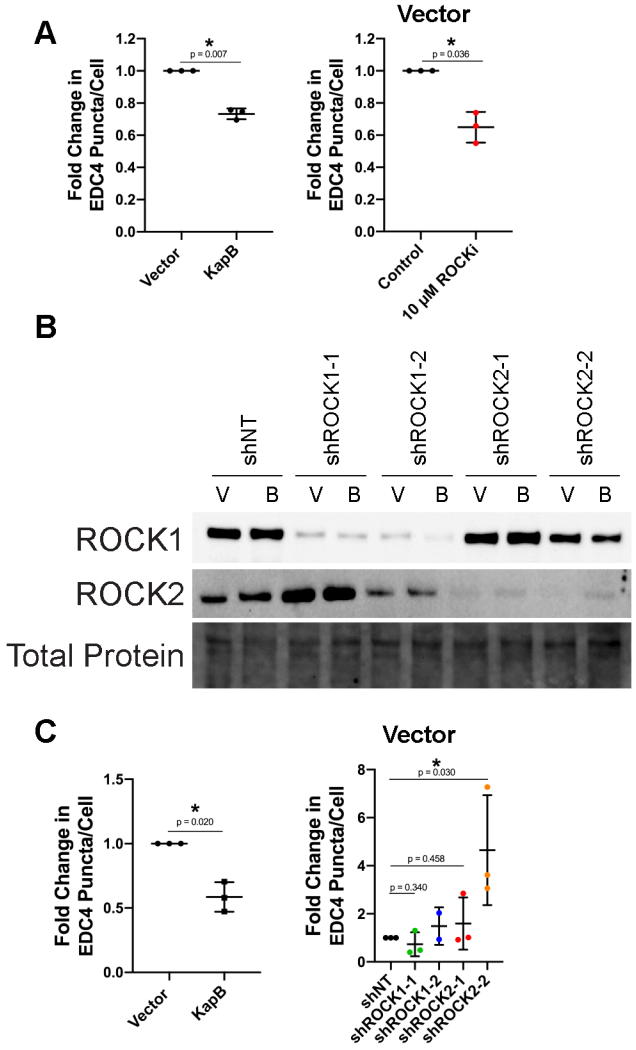
A
Vector
Fold Change in EDC4 Puncta/Cell
p = 0.007
p = 0.036
Vector
KapB
Control
10 μM ROCKi
B
shNT
shROCK1-1
shROCK1-2
shROCK2-1
shROCK2-2
V B V B V B V B V B
ROCK1
ROCK2
Total Protein
C
Vector
Fold Change in EDC4 Puncta/Cell
p = 0.020
p = 0.030
p = 0.458
p = 0.340
Vector
KapB
shNT
shROCK1-1
shROCK1-2
shROCK2-1
shROCK2-2

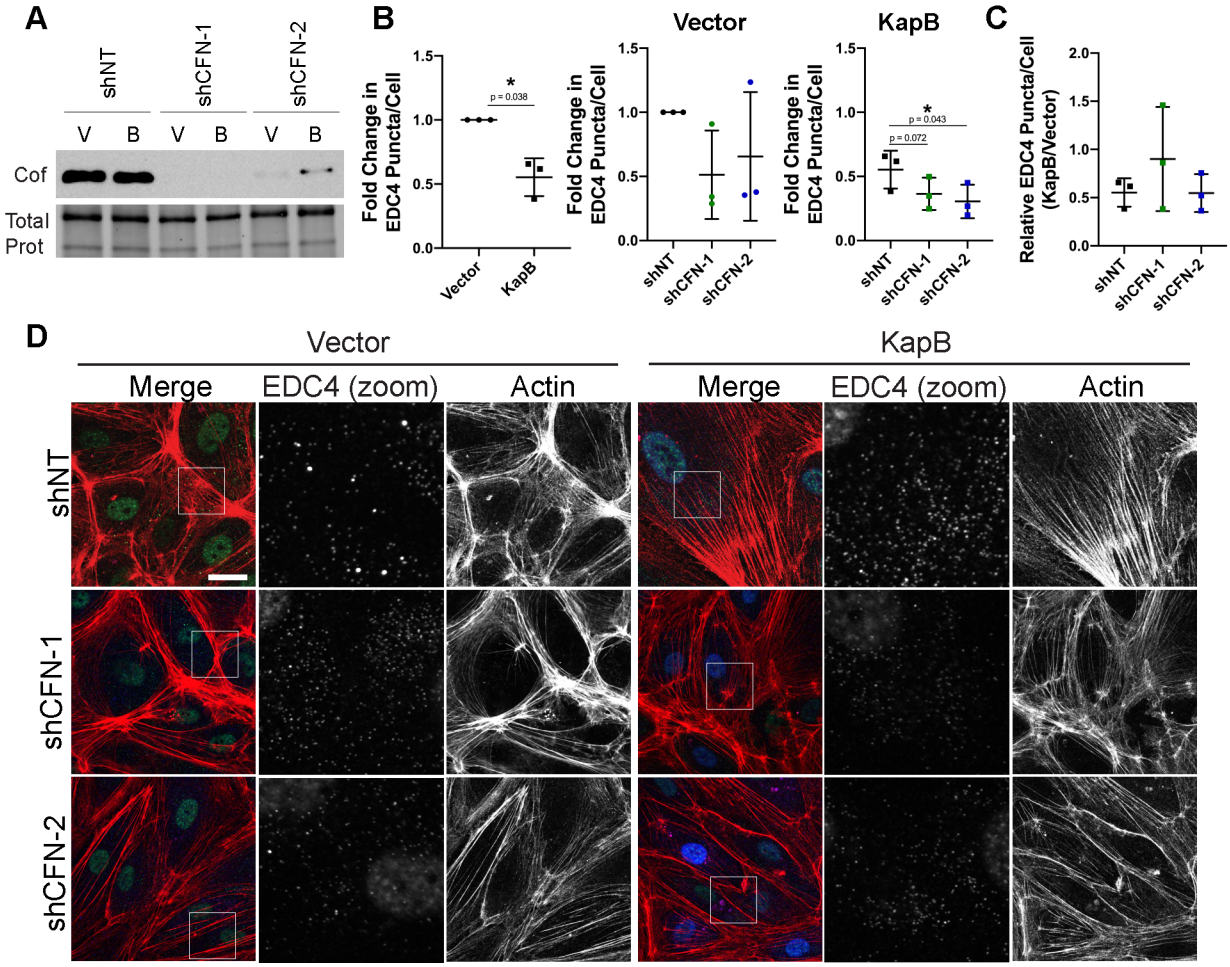
A
shNT
shCFN-1
shCFN-2
V B V B V B
Cof
Total Prot
B
Fold Change in EDC4 Puncta/Cell
p = 0.038
Vector
KapB
Vector
KapB
p = 0.043
p = 0.072
shNT
shCFN-1
shCFN-2
C
Relative EDC4 Puncta/Cell (KapB/Vector)
D
Vector
KapB
Merge
EDC4 (zoom)
Actin
shNT
shCFN-1
shCFN-2

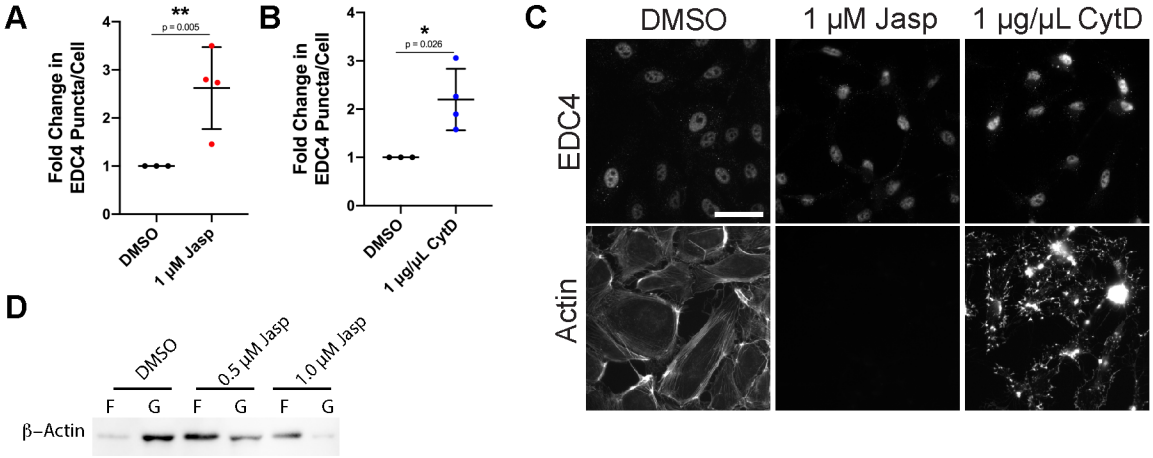
A
**
p = 0.005
Fold Change in EDC4 Puncta/Cell
DMSO
1 μM Jasp
B
*
p = 0.026
Fold Change in EDC4 Puncta/Cell
DMSO
1 μg/μL CytD
C
DMSO
1 μM Jasp
1 μg/μL CytD
EDC4
Actin
D
DMSO
0.5 μM Jasp
1.0 μM Jasp
F G F G F G
β–Actin

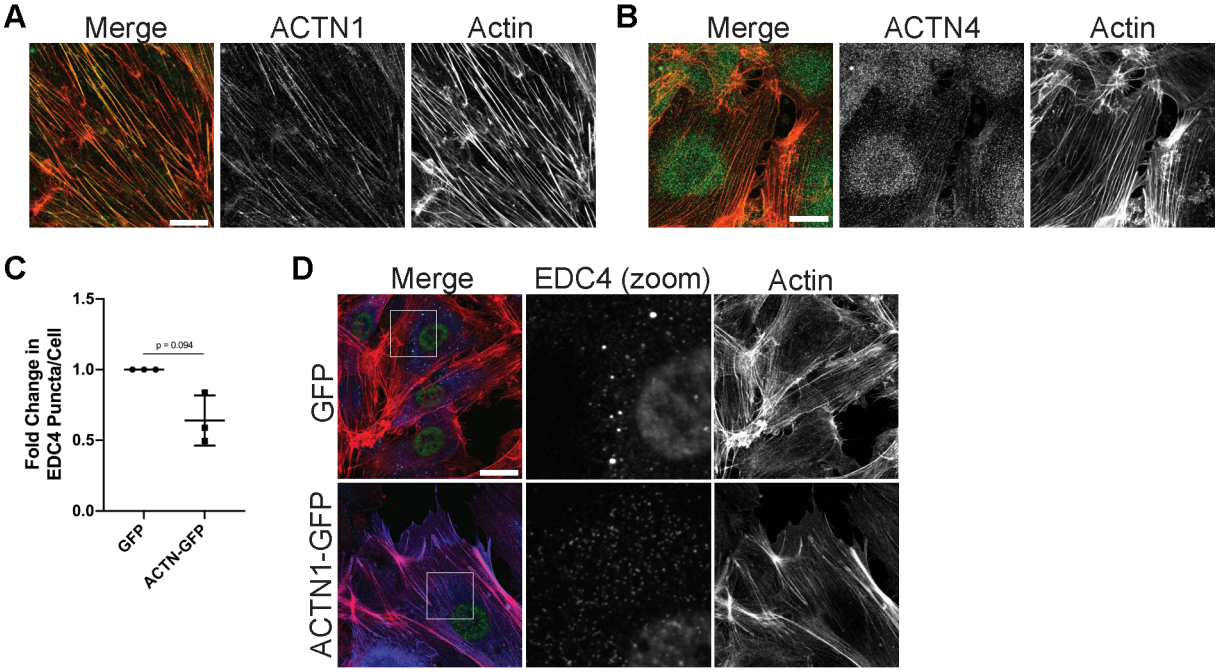
A
Merge
ACTN1
Actin
B
Merge
ACTN4
Actin
C
Fold Change in EDC4 Puncta/Cell
1.5
1.0
0.5
0.0
p = 0.094
GFP
ACTN-GFP
D
Merge
EDC4 (zoom)
Actin
GFP
ACTN1-GFP

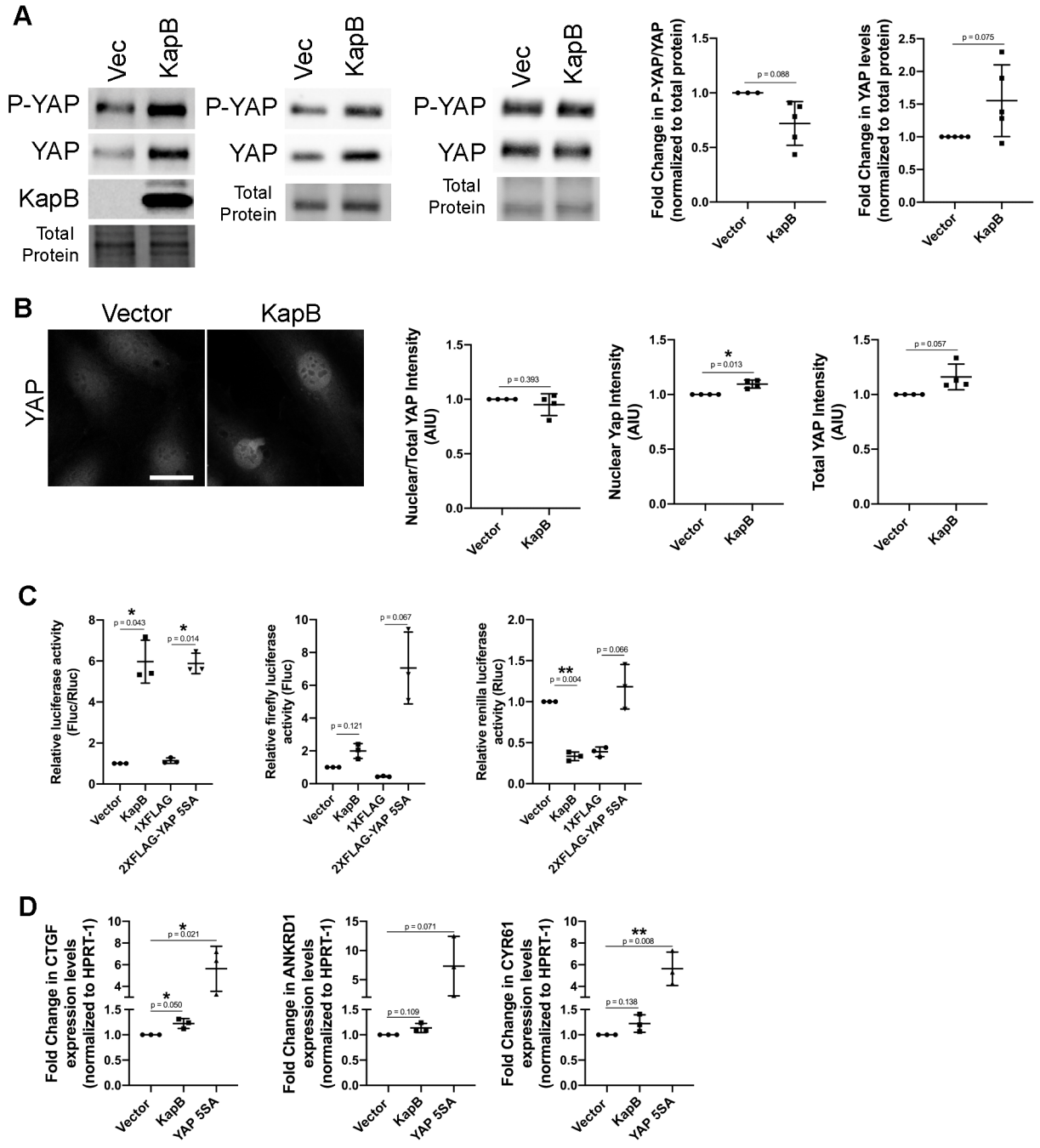
A
Vec
KapB
P-YAP
YAP
KapB
Total Protein
Fold Change in P-YAP/YAP (normalized to total protein)
p = 0.088
Fold Change in YAP levels (normalized to total protein)
p = 0.075
Vector
KapB
B
Vector
KapB
YAP
Nuclear/Total YAP Intensity (AIU)
p = 0.393
Nuclear Yap Intensity (AIU)
p = 0.013
Total YAP Intensity (AIU)
p = 0.057
C
Relative luciferase activity (Fluc/Rluc)
p = 0.043
p = 0.014
Relative firefly luciferase activity (Fluc)
p = 0.121
p = 0.067
Relative renilla luciferase activity (Rluc)
p = 0.004
p = 0.066
Vector
KapB
1XFLAG
2XFLAG-YAP 5SA
D
Fold Change in CTGF expression levels (normalized to HPRT-1)
p = 0.021
p = 0.050
Fold Change in ANKRD1 expression levels (normalized to HPRT-1)
p = 0.071
p = 0.109
Fold Change in CYR61 expression levels (normalized to HPRT-1)
p = 0.008
p = 0.138
Vector
KapB
YAP 5SA

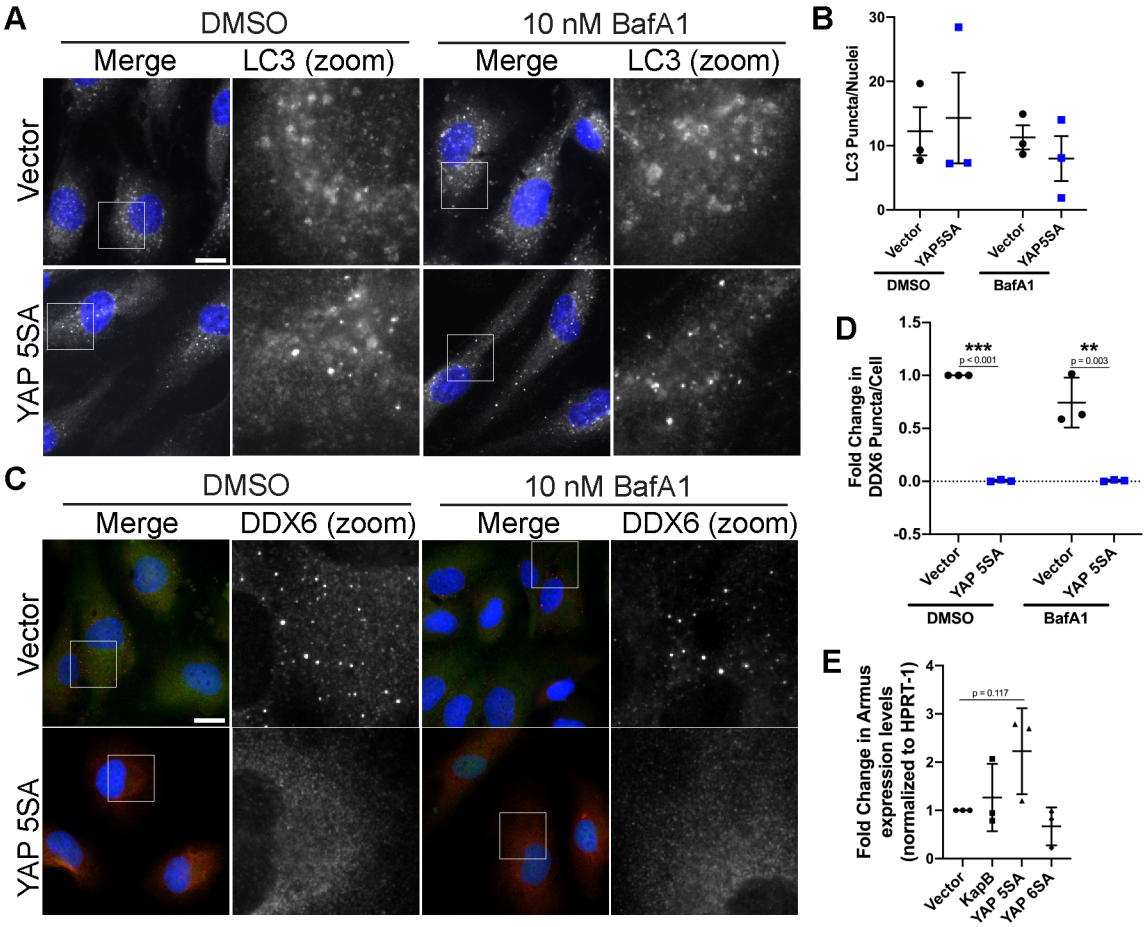
A
DMSO
10 nM BafA1
Merge
LC3 (zoom)
Merge
LC3 (zoom)
Vector
YAP 5SA
B
LC3 Puncta/Nuclei
30
20
10
0
Vector
YAP5SA
Vector
YAP5SA
DMSO
BafA1
C
DMSO
10 nM BafA1
Merge
DDX6 (zoom)
Merge
DDX6 (zoom)
Vector
YAP 5SA
D
Fold Change in DDX6 Puncta/Cell
1.5
1.0
0.5
0.0
-0.5
***
p < 0.001
**
p = 0.003
Vector
YAP 5SA
Vector
YAP 5SA
DMSO
BafA1
E
Fold Change in Armus expression levels (normalized to HPRT-1)
4
3
2
1
0
p = 0.117
Vector
KapB
YAP 5SA
YAP 6SA